Title
Anaerobic microbial activity affects earliest diagenetic pathways of bivalve shells

Journal
Sedimentology, 65(4)

ISSN
0037-0746

Authors
Lange, Skadi M
Krause, Stefan
Ritter, Ann-Christine
et al.

Publication Date
2018-06-01

DOI
10.1111/sed.12428

Peer reviewed

SEDIMENTOLOGY the journal of the International Association of Sedimentologists

Sedimentology (2018) doi: 10.1111/sed.12428

Anaerobic microbial activity affects earliest diagenetic pathways of bivalve shells

SKADI M. LANGE*, STEFAN KRAUSE*, ANN-CHRISTINE RITTER†, VANESSA FICHTNER‡, ADRIAN IMMENHAUSER†, HARALD STRAUSS‡ and TINA TREUDE§¶

**Department of Biogeochemistry, GEOMAR Helmholtz Centre for Ocean Research Kiel, Wischhofstr. 1-3, 24148 Kiel, Germany (E-mail: sklange@geomar.de)*

†Department of Geology, Mineralogy, and Geophysics, Ruhr-University Bochum, Universitätsstr. 150, 44801 Bochum, Germany

‡Department of Geology and Paleontology, University of Münster, Corrensstr. 24, 48149 Münster, Germany

§Department of Earth, Planetary, and Space Sciences, University of California, Los Angeles, 595 Charles E. Young Drive, Los Angeles, CA 90095-1567, USA

¶Department of Atmospheric and Oceanic Sciences, University of California, Los Angeles, 595 Charles E. Young Drive, Los Angeles, CA 90095-1567, USA

Associate Editor – Giovanna Della Porta

ABSTRACT

The earliest diagenetic post-mortem exposure of biogenic carbonates at the sea floor and in the uppermost sediment column results in the colonization of hard-part surfaces by bacterial communities. Some of the metabolic redox processes related to these communities have the potential to alter carbonate shell properties, and hence affect earliest diagenetic pathways with significant consequences for archive data. During a three-month *in vitro* study, shell subsamples of the ocean quahog *Arctica islandica* (Linnaeus, 1767) were incubated in natural anoxic sediment slurries and bacterial culture medium of the heterotrophic *Shewanella sediminis* HAW-EB3. Bulk analyses of the liquid media from the *Shewanella sediminis* incubation revealed an over ten-fold increase in total alkalinity, dissolved inorganic carbon and $\Omega_{Aragonite}$, and the alteration of the Mg/Ca, Mg/Sr and Sr/Ca ratios relative to control incubations without cultures. Ion ratios were most affected in the incubation with anoxic sediment, depicting a 25% decrease in Mg/Ca relative to the control. Shell sample surfaces that were exposed to both incubations displayed visible surface dissolution features, and an 8 wt% loss in calcium content. No such alteration features were detected in control shells. Apparently, alteration of shell carbonate properties was induced by microbially driven decomposition of shell intercrystalline organic constituents and subsequent opening of pathways for pore fluid–crystal exchange. This study illustrates the potential influence of benthic bacterial metabolism on biogenic carbonate archives during the initial stages of diagenetic alteration within a relatively short experimental duration of only three months. These results suggest that foremost the biological effect of bacterial cation adsorption on divalent cation ratios has the potential to complicate proxy interpretation. Results shown here highlight the necessity to consider bacterial metabolic activities in marine sediments for the interpretation of palaeo-environmental proxies from shell carbonate archives.

Keywords Alteration, aragonite, bacteria, carbonate, diagenesis.

INTRODUCTION

Marine biogenic carbonates represent one of the most important archives in palaeo-environmental reconstruction (Dodd, 1963; Williams *et al.*, 1982; Wilson & Opdyke, 1996; Schöne, 2013; Immenhauser *et al.*, 2016). After deposition on the sea floor, these archives are subject to diagenetic processes including organic matter degradation and neomorphism, as well as isotopic and elemental exchange with the environment. Traditionally, research on early carbonate ($CaCO_3$) diagenesis in the marine realm has primarily focused on abiotic factors (Bathurst, 1975; Berner, 1980; Swart, 2015). Clearly, this approach has limitations in capturing all potential effects of early diagenesis, because carbonates in marine sediments are exposed to microbial metabolic activities that are acknowledged (Walker, 1984; Nealson, 1997; Vasconcelos & McKenzie, 1997; Riding, 2000) but often not considered in detail. For example, microbial micritization of skeletal and non-skeletal carbonates is known to contribute to carbonate alteration (Tucker & Bathurst, 1990), and was found to influence stabilization and cementation of shallow carbonate sands (Hillgärtner *et al.*, 2001).

Organic matter in marine sediments is subject to a succession of heterotrophic microbial metabolisms, which are thermodynamically organized along the Gibbs free energy yield (Froelich *et al.*, 1979; Jørgensen, 2006; Orcutt *et al.*, 2011). Metabolic products resulting from these processes can shift the (micro-) environmental chemistry to acidic or alkaline conditions and support carbonate dissolution or secondary carbonate nucleation, respectively (Sotaert *et al.*, 2007). For example, corrosion of shell carbonate was detected at the oxic–anoxic boundary layers of hydrocarbon seeps as a result of microbial aerobic oxidation (Cai *et al.*, 2006; Himmler *et al.*, 2011) and a wide range of microbial metabolic activity facilitates carbonate precipitation (Greenfield, 1962; Chafetz & Buczynski, 1992; Dupraz *et al.*, 2004; Wright & Wacey, 2005; Sánchez-Román *et al.*, 2007).

Numerous studies report the direct attachment of bacterial cells to minerals through extracellular polymeric substances (EPS), which predominantly consist of polysaccharides (Sutherland, 2001). The attachment subsequently leads either to mineral weathering (Paine *et al.*, 1933; Decho *et al.*, 2005; Uroz *et al.*, 2009; Krause *et al.*, 2014), excavation and etch pit formation (Davis *et al.*, 2007), or on the contrary to the inhibition of etch pit formation and mineral dissolution through detection of carbonate high energy sites (Lüttge *et al.*, 2005). Furthermore, microbial biofilm EPS functions either as a precipitation-facilitating microenvironment (Aloisi *et al.*, 2006) or, in contrast, as an inhibitor of precipitation (Decho, 2010). Kawaguchi & Decho (2002) experimentally tested the influence of EPS on carbonate polymorphism, where partly lithified layers of EPS from a microbial stromatolite induced calcite crystal formation, while unlithified EPS layers induced the formation of aragonite.

Many bacteria are capable of divalent cation complexation (Beveridge & Murray, 1980; Konhauser *et al.*, 1993), and the EPS of sulphate-reducing bacteria (SRB) was reported to specifically bind calcium ions (Braissant *et al.*, 2007). The latter group is known to induce carbon isotope fractionation (Londry & Des Marais, 2003), and evidence for a two-step fractionation process in Ca isotopes by non-stoichiometric dolomite-precipitating SRB has recently been provided by Krause *et al.* (2014). Furthermore, cation complexation by functional groups of Gram-negative bacterial cell wall lipopolysaccharides (LPS) was confirmed in previous studies (Schindler & Osborn, 1979; Coughlin *et al.*, 1983; Selvarengan *et al.*, 2010). These findings demonstrate the necessity for an improved understanding of microbially induced carbonate alteration in marine sediments during the earliest diagenetic stages.

Given its great diversity in marine sediments, microbial activity has the potential to alter primary morphology, mineralogy and chemistry, as well as isotopic and elemental composition of biogenic carbonate archives, thereby possibly affecting palaeo-environmental proxies. Alteration can be induced in two manners: (i) by microbial 'mining' for intrashell organic matter (both intercrystalline and intracrystalline) with all related dissolution, reprecipitation and neomorphic processes; and (ii) by increasing the shell reactive surface of carbonate archives. The latter process takes place via the disintegration of intercrystalline organic matter, thus creating pathways and enhancing fluid–carbonate reaction rates.

In this study, a three-month *in vitro* experiment was conducted, during which shell subsamples of the bivalve *Arctica islandica* were incubated in either anoxic seawater medium that contained the marine benthic bacterial strain *Shewanella sediminis* HAW-EB3 or anoxic

slurries of natural marine sediment. *Arctica islandica* is a widely used archive for reconstructing the more recent climate dynamics with a focus on the North Atlantic domain. It is the longest living non-colonial animal with a potential lifespan of over 500 years (Abele *et al.*, 2008; Butler *et al.*, 2013). Passive diffusion and uptake of seawater and carbonate ions as well as the active transport of Ca^{2+} and Sr^{2+} into *A. islandica* hemolymph result in shell carbonate precipitation in near isotopic equilibrium with its environment (Schöne, 2013; Shirai *et al.*, 2014). The endobenthic, burrowing lifestyle of *A. islandica* accounts for immediate post-mortem exposure to pore fluids and related earliest diagenetic processes.

Out of the many bacterial species with metabolic carbonate-alteration potential *S. sediminis* HAW-EB3 (Zhao *et al.*, 2005), a facultative anaerobic, gram-negative, heterotrophic bacterium was chosen for the bacterial culture incubation. As a psychrophilic organism, first isolated from marine sediments off the coast of Halifax, NS, Canada, *S. sediminis* is a representative of cold-adapted bacteria. This organism is capable of oxidizing and fermenting N-acetylglucosamine (Zhao *et al.*, 2005), an integral constituent of the bivalve shell intercrystalline and intracrystalline organic matrix (Watabe, 1965; Weiner & Addadi, 1991; Marin, 2012). While the bacterial culture allowed for distinct experimental effects that could be assigned to a single bacterial species with fermentative metabolic activity, the *in vitro* sediment incubation represented an anoxic sediment system with a natural anaerobic benthic microbial community that could foster carbonate precipitation processes through metabolic generation of alkalinity.

In the context of this study, the following research questions were addressed: (i) do microbial metabolic processes in marine sediments alter biogenic carbonates during sea floor and shallow burial processes; (ii) if so, are alteration processes recorded in crystal ultrastructure and mineralogy, chemistry and isotopic composition of biogenic carbonates; and (iii) if so, does microbial activity affect the diagenetic stability of carbonate (here specifically aragonite) archives?

Work presented here is of significance for those concerned with the interpretation of proxy data from marine carbonate archives in general and sheds light on microbe–carbonate interaction in the earliest marine pore water diagenetic realm.

METHODS

Seawater medium and bacterial culturing

All incubations were carried out in media using modified natural, fully marine seawater from the North Sea. The seawater was sampled south-east of Heligoland (54°06′N, 008°00′E) during *R/V Heincke* cruise HE-411. The seawater was stored in a bulk container (IBC) at 10°C and circulated with an EHEIM compact 600 aquarium pump (EHEIM, Deizisau, Germany) to allow for steady oxygenation. Seawater aliquots for the experiment were sterilized with a UV water sterilizer (Wiegandt GmbH, Krefeld, Germany), followed by filtration through a 0·2 μm Whatman Polycap™ 75 AS Filter (GE Healthcare Life Sciences, Buckinghamshire, UK).

Shewanella sediminis HAW-EB3 was obtained from the Leibniz Institute DSMZ – German Collection of Microorganisms and Cell Cultures (Braunschweig, Germany). The culture was grown at 10°C in DSMZ medium 514 with the following composition (g l^{-1}): peptone, 5·0; yeast extract for bacterial media (Carl Roth, Karlsruhe, Germany), 1·0; Fe(III) citrate, 0·1; NaCl, 19·45; $MgCl_2{\cdot}6H_2O$, 12·6; Na_2SO_4, 3·24; $CaCl_2{\cdot}2H_2O$, 2·39; KCl 0·55; $NaHCO_3$, 0·16; KBr, 0·08; $SrCl_2$, 0·034; H_3BO_3, 0·022; NaF, 0·0024; $(NH_4)NO_3$, 0·0016; $Na_2HPO_4{\cdot}2H_2O$, 0·01; and 2·9 μl Na-silicate (Table 1). Medium pH was adjusted to 7·6 with 1 M NaOH. Prior to inoculation, sterile culturing vials and medium were purged with N_2/CO_2 gas (80%/20%). From the

Table 1. Composition of the bacterial culture medium.

Component	g l^{-1}
Peptone	5·00
Yeast extract	1·00
Fe(III) citrate	0·10
NaCl	19·45
$MgCl_2{\cdot}6H_2O$	12·60
Na_2SO_4	3·24
$CaCl_2{\cdot}2H_2O$	2·39
KCl	0·55
$NaHCO_3$	0·16
KBr	0·08
$SrCl_2$	0·034
H_3BO_3	0·022
Na-silicate	0·004
NaF	0·0024
$(NH_4)NO_3$	0·0016
$Na_2HPO_4{\cdot}2H_2O$	0·01

third generation on, the *S. sediminis* culture was inoculated to sterile seawater medium containing 100 mg l^{-1} additional Fe (III) citrate, 1000 mg l^{-1} yeast and 200 μl resazurin as redox/oxygen indicator. Seawater medium was purged with N_2 and 900 ml was transferred to a sterile 2 l gastight flat flange beaker with a final 1100 ml N_2 headspace of 0·2 bar above atmospheric pressure. At the experimental start, 10 ml of the *S. sediminis* culture was inoculated into the medium. Controls included the bacteria-free sterile seawater medium containing 100 mg l^{-1} additional Fe (III) and 1000 mg l^{-1} yeast with 200 μl sterile resazurin. Both incubations were kept at 10°C during the whole experiment.

Anoxic sediment slurries

Anoxic sediment samples were obtained with *R/V Suedfall* from Piep, Büsum (German Bight; 54°50′N, 8°89′E), at 17 m water depth with a Van Veen grab sampler. These sediments are generally characterized by an alternating mixture of clay, silt and sand. The carbonate content in the sediments ranges between 0·9% (*ca* at sampling depth) and *ca* 15%, and the share in quartz is up to 90% in the mean (Pratje, 1932; Little-Gadow, 1982). Samples were extricated from organic debris and subsequently stored at 0·9°C in sterile 1 l Duran flasks that were closed with sterilized butyl rubbers. Slurries were prepared from sediment and sterile seawater (1 : 2) in sterile 2 l gastight flat flange beakers with a 1100 ml N_2 headspace of 1 bar above atmospheric pressure. Controls contained sediment and sterile seawater (1 : 2) without shell samples. Sterile resazurin (220 μl) was added to each incubation.

Bivalve shells

Arctica islandica bivalves were dredged alive in 2010 from the sea floor off north-east Iceland at water depths between 40 m and 120 m for commercial purposes. Valves were disposed on shell mittens where they were collected briefly after disposal. Shells of adult specimens (*ca* 70 years) with approximately the same shell heights (distance umbo–ventral margin of *ca* 10 cm) and valve thickness (2 to 5 mm) were selected for the alteration experiments. The maximum valve length of *A. islandica* is reported to reach approximately 13 cm. Note that growth rates of bivalves differ between specimens and bivalves with near-identical dimensions are not *a priori* of the same ontogenic age. Based on sclerochronological data, the age differences between specimens used in this study were estimated to be 10 years or less. Each of the selected valves was cleaned and divided into two halves using a thin diamond saw. Subsequently, a *ca* 2·5 cm wide longitudinal shell section including portions of the central axis of the bivalve and the hinge was cut from one of the half valves. This longitudinal section was then cut into *ca* 8 to 10 subsamples of similar dimensions, depending on the respective valve size. The subsamples were further sawn to approximately 1·0 × 1·0 × 0·5 cm sized pieces for the alteration experiments (Fig. 1), and all available shell parts

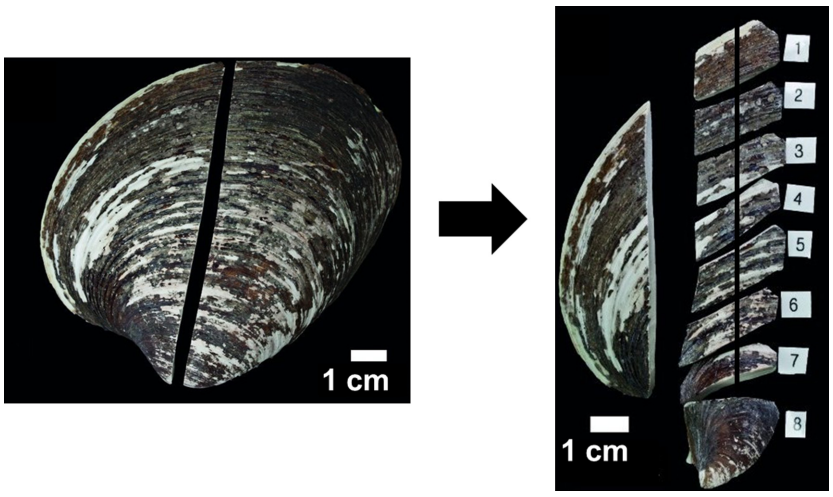

Fig. 1. Scheme of shell sample division. Valves were first cut in half and subsequently subdivided for the incubations (modified after Ritter *et al.*, 2017).

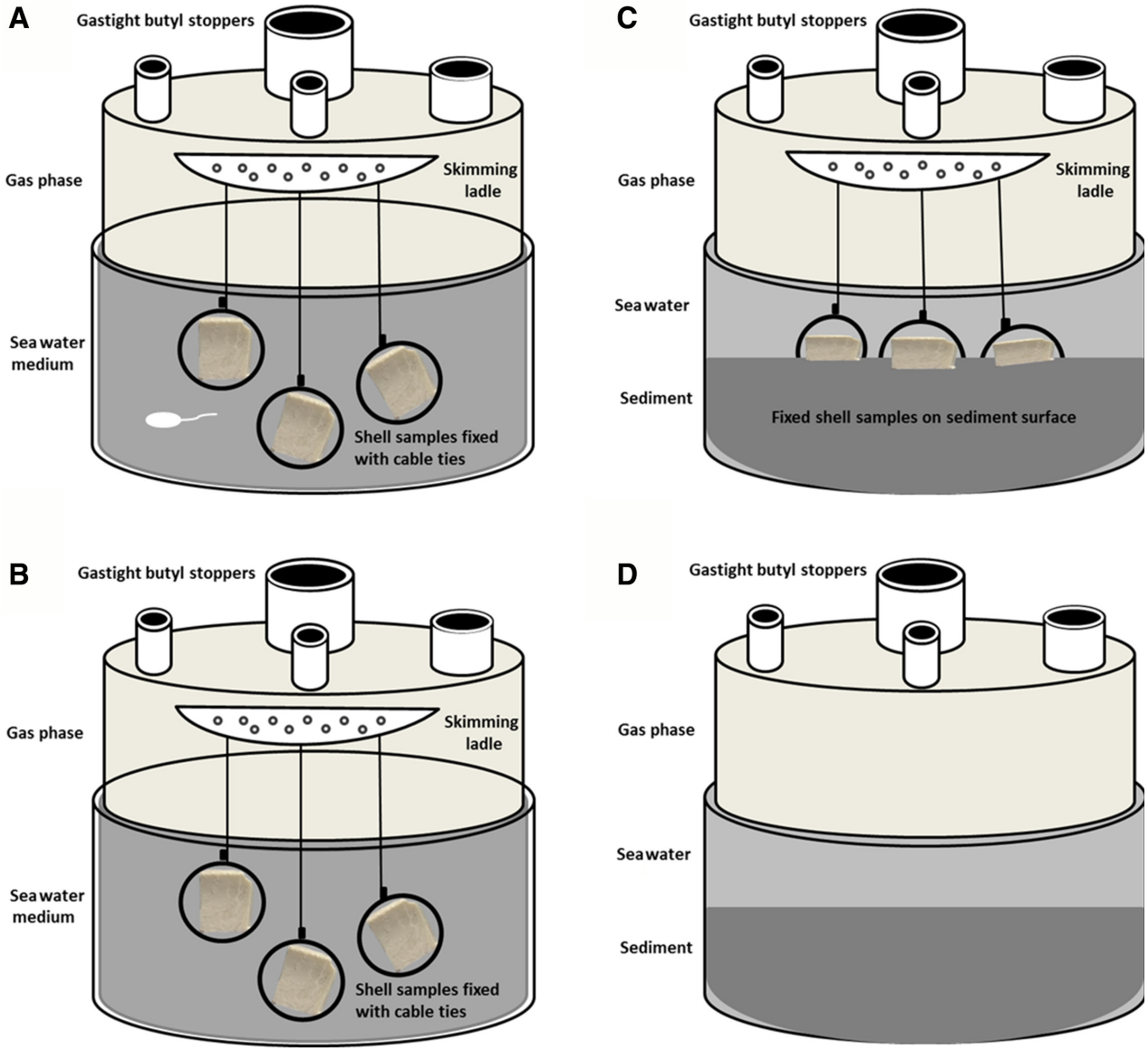

Fig. 2. Sketch of the incubation set-ups: (A) the *S. sediminis* culture; (B) the cell-free control; (C) the anoxic sediment; and (D) the sediment control. In the upper top of a gastight flat flange beaker, an inert skimming ladle, with the handle removed, serves as mounting for shell samples that are fixed with cable ties and hung into the medium/deposited on the sediment via threads.

except for the umbo regions were used for the incubations.

Incubation procedure and post-incubation treatment

Shell sample edges were fixed with sterile plastic cable ties. Inert Teflon-skimming ladles, with the handles removed, were used to attach sewing threads of differing lengths that were knotted to the cable ties and allowed for free distribution of samples in sterile 2 l flat flange beakers (Fig. 2). Samples were hung in the *S. sediminis* culture medium, respectively, or deposited on the sediment surface. Flat flange beakers were smoothly pivoted every other day to mimic natural seawater movement. After an incubation period of 101 days at 10°C in the dark, samples were carefully rinsed with sterile seawater, followed by ultra-purified water with a pH adjusted to *ca* 8 with NH_4^+-solution. Samples were dried in parafilm-sealed Petri dishes at a temperature of 40°C and then stored at room temperature for upcoming analyses. Liquids from the shell-cleaning

procedure (*ca* 2 ml each) were preserved in formalin (final concentration 2%) at 4°C. For cell staining and analysis, 100 μl of each liquid sample was transferred to 5 ml 1× sterile PBS and filtered on a 0·2 μm Whatman™ Nucleopore™ polycarbonate membrane filter (GE Healthcare, 37586 Dassel). The filters were dried at room temperature, embedded in 1% low-melt agarose and dried at 37°C. Staining of the filters was conducted with 4,6 diamidino-2-phenylindole (DAPI) solution (1 μl ml^{-1}) for 15 min in the dark and filters were transferred to microscope slides. A drop of antifading agent (CitiFluor AF-1 solution) was placed on the filter before sealing with a cover slip. The slides were examined and photographed with a Zeiss Axio Imager.M2 stereomicroscope, using a DAPI filter set, and imaging was carried out with the ZEN Pro 2012 software (Carl Zeiss Microscopy GmbH, Jena, Germany).

Carbonate system and geochemistry of seawater media

Measured carbonate system parameters were pH, total alkalinity (TA) and dissolved inorganic carbon (DIC). Sampling for all parameters was conducted on a regular basis (daily to weekly). The pH was measured with a Schott Instruments Lab 850 pH sensor (SI Analytics GmbH, Mainz, Germany). The pH sensor was calibrated with reference solution buffers (L4794, L4796, L4799, SI Analytics GmbH) according to the Physikalisch-Technische Bundesanstalt (PTB) and the National Institute of Standards and Technology (NIST). Measurements of pH and TA were taken on 12 ml medium aliquots in sterile 50 ml Duran® flasks under aerobic conditions. The pH measurement was conducted directly after sampling on the whole 12 ml aliquot. As the Duran® flasks had to be opened during the measurements, the measuring time was restricted to 20 sec per sample to keep the equilibration of anoxic samples with the ambient atmosphere minimal. Subsequently, the 12 ml aliquots were sterile-filtered and all subsamples for analyses were taken from the bulk fluid. Total alkalinity was determined via open-cell titration of 0·5 ml samples with 0·01 M HCl in a titration vessel after Pavlova (Pavlova *et al.*, 2008), using a Metrohm 876 Dosimat plus (Ω Metrohm, Riverview, FL, USA). During titration, the vessel was continuously purged with N_2 to strip CO_2 released by acid addition. All TA measurements were calibrated with IAPSO seawater standard. For DIC measurements, 1·8 ml samples were treated with 10 μl $HgCl_2$ saturated solution in a 2 ml glass vial, crimp-sealed and stored at 4°C for further processing. The DIC concentration was determined as CO_2 with a Multi N/C 2100 Analyzer (Analytik Jena, Jena, Germany). The detection limit was 0·1 ppm with a precision of 2%. The pCO_2 and the saturation state of aragonite ($\Omega_{Aragonite}$) were calculated on the basis of measured pH and DIC concentrations after Zeebe & Wolf-Gladrow (2001) with MATLAB®. For minor and trace element concentrations, 1 ml medium samples were acidified with 0·1 ml HNO_3 Suprapur© (1/100 v/v) in a 2 ml cryo vial and stored at 4°C for further processing. Divalent cation concentrations were measured by inductively coupled plasma – atomic emission spectroscopy (ICP–AES – JY 170 ULTRATRACE; HORIBA Limited, Kyoto, Japan). The detection limit was 2 mg l^{-1} for Ca^{2+}, 6 mg l^{-1} for Mg^{2+} and 25 μg l^{-1} for Sr^{2+}, with a precision of 2%.

Shell structure and elemental composition

All incubated shell samples were examined with a Leica M 165 FC binocular stereomicroscope (Leica AG, Wetzlar, Germany) prior to and after incubation, and pictures were generated using Leica AS software. Raman spectroscopy was conducted on one sample per incubation type prior to and after incubation with a LabRAM HR800 spectrometer (Horiba Jobin Yvon GmbH, Bensheim, Germany). Samples were analysed at room temperature and studied without pre-treatment. Along a transect of 1 cm, the carbonate was excited with the 473 nm line of a Nd-YAG laser. Scattered radiation from the samples was measured in a 90° scattering geometry. The Raman spectra were obtained at an interval of 0·65 cm^{-1} (0 to 4000 cm^{-1}) and a slit width of 100 mm. Scanning electron microscopy (SEM) and electron microprobe (EMP) mapping were applied post-incubation to one sample of each incubation type, the respective controls and a non-incubated shell sample each, with a JEOL JXA 8200 Electron Probe Microanalyzer (JEOL Limited, Tokyo, Japan). For SEM analyses, sample surfaces were air-dried and sputter-coated using a platinum/gold target. The SEM images were acquired at 15 kV and a 19 μA filament current.

Prior to the EMP mapping, shell samples were sawn into quarters, and the sawn surface of one quarter each was ground using Hermes water

grinding papers (P1200, P2400 and P4000) at a pressure of 25 N. Each grinding step was followed by drying and cleaning of the sample with pressurized air. Samples were subsequently embedded in epoxy resin (Araldite® 2020; Huntsman Corporation, The Woodlands, TX, USA) and dried overnight at 50°C. Electron microprobe mapping was applied to determine element distribution in relation to the surface structures observed by SEM. The maps were obtained by wavelength dispersive spectrometry (WDS) mode and repeated to gather eight accumulations of the selected area. Standards (calcite, KAN1, VG-2, strontianite A2_modernCoral) were measured prior and after mapping to calculate trace element concentrations. For quantitative wavelength dispersive analyses, the element concentrations were subsequently measured along a mapping area of 600 μm parallel to the exposed rim of the sample $\times$ 300 μm in the direction of non-exposed, inner sample parts, simultaneously measuring Mg (TAP, Ka), Sr (TAP, strontianite), Ca (PETJ), P (PETH) and S (PETH). The measurements were conducted at a beam current of 50 nA with a beam spot size of 3 μm. Accelerating voltage was set to 15 kV.

Micro-X-ray fluorescence (μ-XRF) mapping of Sr^{2+} was conducted at the PHOENIX beamline (Paul Scherrer Institute, Switzerland). Prior to the analyses, the samples were cut parallel to the growth direction and mounted on a glass holder in order to perform element mapping along a transect from the inner to the outer shell rim. The thin sections were polished to a thickness of 200 μm. During measurements, a fixed Si (111) monochromator (Bruker ACCEL, Bremen, Germany) with an energy resolution higher than 0·5 eV was used. Fluorescence signals were collected with a detector equipped with four elements of silicon drift diodes (VORTEX, USA). With a beam energy of 2800 eV, the strontium L-edge electrons were excited to display the strontium distribution in the shell samples. Contemporary detection of phosphorus K-edge electrons allowed for discrimination between phosphorus-rich resin (Körapox 439; Kömmerling, Pirmasens, Germany) and phosphorus-poor *A. islandica* shell. The element maps were generated with a spatial resolution of 5 μm.

Carbon and oxygen isotope analyses

Following incubation, *A. islandica* shell material was sampled for its carbon ($\delta^{13}C$) and oxygen ($\delta^{18}O$) isotopic values. Samples were retrieved from one incubated shell block per incubation type. Sample material was scratched off with a scalpel directly beneath the outer organomineralic (periostracal), and from outer and inner biomineralic (aragonitic) parts of the shell (see Ritter *et al.*, 2017, for a detailed description of the sampling procedure), as well as from all surfaces of subsamples exposed to the ambient medium (Table 3). A total of 0·4 $\pm$ 0·04 mg of the subsample was transferred into glass vials and dried at 105°C for 48 h. The glass vials were then closed gastight and transferred into an autosampling device at 70°C. The atmosphere within the vials was removed by flushing with helium gas and a few drops of phosphoric acid were added to the sample. Carbon and oxygen isotope values were subsequently measured from the liberated CO_2 gas using a Thermo Finnigan MAT253 mass spectrometer (Thermo Fisher Scientific Inc., Waltham, MA, USA) interfaced to a GasBench. Carbon and oxygen isotope results are given in ‰ relative to the VPDB (Vienna Pee Dee Belemnite) standard. For correction of the measured data, international standards CO1, CO8 and NBS-19 as well as an in-house standard have been measured in addition to the samples.

RESULTS

Seawater medium

During all incubations, no colour change in the added resazurin/resorufin indicator from colourless (anoxic conditions) to pink (partially or fully oxic conditions) was observed, confirming continuous anoxic conditions. Clear trends were observed in pH, TA and $\Omega_{Aragonite}$, and divalent cation ratios in the medium chemistry of both the *S. sediminis* incubation and the anoxic sediment. The cell-free medium control featured fluctuating values in all measured parameters potentially due to imprecise pipetting of small aliquots, but showed no trend in the development of any of the parameters over time. The increasing pH, TA and $\Omega_{Aragonite}$ in the sediment control reflected natural anoxic sediment conditions with live bacterial communities, and no trend in medium divalent cation concentration and/or ratios was observed.

Total alkalinity (TA), DIC and $\Omega_{Aragonite}$ in both incubation media containing shells increased markedly during the incubation period (Figs 3 and 4). The initial pH of 7·3 in the *S. sediminis* culture medium decreased to 7·1

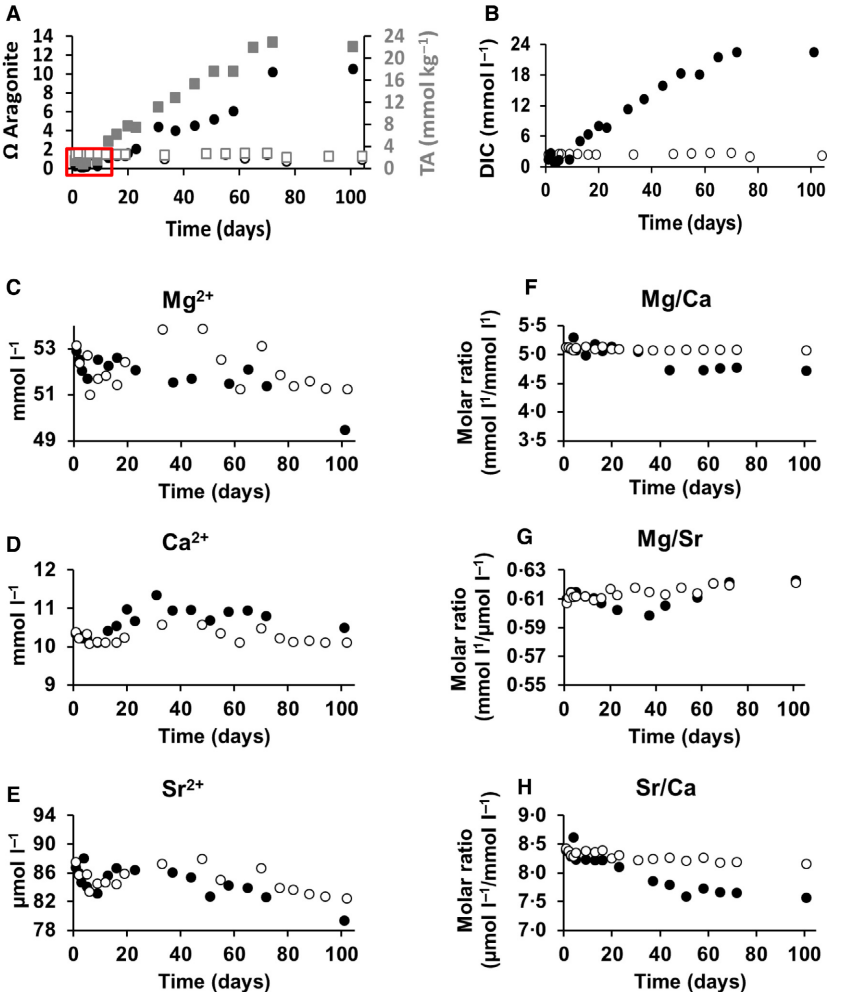

Fig. 3. Medium chemistry of the *S. sediminis* incubation: temporal development of (A) $\Omega_{Aragonite}$ (circles) and total alkalinity (TA) (squares); (B) dissolved inorganic carbon (DIC); (C) to (E) divalent cation concentrations; and (F) to (H) divalent cation ratios. Solid symbols show bulk-medium values, and open symbols show control values. Note the $\Omega_{Aragonite}$ undersaturation at the experiment start, as well as the general variation in the cation control concentrations, apparently caused by errors occurring due to imprecise pipetting of small aliquots.

on day four and increased to 7·6 on day 31. After a decrease to pH 7·5, the pH increased to values between pH 8 and pH 7·7 at the end of the experiment (Table 2). Total alkalinity increased from 1·8 to 22·8 mmol kg^{-1} over the entire incubation period. Undersaturation with respect to aragonite at the experimental start was followed by an increase in $\Omega_{Aragonite}$ from 1·1 to 10·2 (Fig. 3A). The dissolved inorganic carbon (DIC) increased from 1·4 to 22·5 mmol l^{-1} (Fig. 3B) and pCO_2 increased from 1463 to 9467 μatm (Table 2). In the anoxic sediment incubation, pH values were fluctuating between 7·7 and 7·9 throughout the experimental duration. Total alkalinity increased from an initial 2·9 to 6·3 mmol kg^{-1}, $\Omega_{Aragonite}$ from 1·9 to 4·9 (Fig. 4A) and DIC concentrations from 2·8 to 6·2 mmol l^{-1} (Fig. 4B). The pCO_2 values were not tightly correlated to pH; the initial pCO_2 of 764 μatm increased to 2080 μatm on day one and varied between 1458 and 2094 μatm until the end of the experiment (Table 2). The Ca^{2+} concentration in the *S. sediminis* culture medium increased from an initial 10·3 to 11·3 mmol l^{-1} on day 31, stayed at values between 10·9 and 10·7 mmol l^{-1} and finally decreased to 10·5 mmol l^{-1} at the very end of the experiment (Fig. 3D). The Mg^{2+} and Sr^{2+} concentrations decreased from an initial 52·9 to 49·5 mmol l^{-1} and from 86·7 to 79·4 μmol l^{-1}, respectively (Fig. 3C and E). Consequently, the Mg/Ca ratio decreased from an initial 5·1 to a constant value of 4·7 at the end of the experiment, and the Sr/Ca ratio decreased from 8·4 to 7·6, while the Mg/Sr ratio slightly increased from 0·61 to 0·62 (Fig. 3F to H). In the anoxic sediment incubation, a strong increase in Ca^{2+} from initial 10·3 to 13·8 mmol l^{-1}, in Mg^{2+} from 52·5 to 53·4 mmol l^{-1} and in Sr^{2+} from 86·4 to 96·8 μmol l^{-1} during the experiment (Fig. 4C to E) led to a decrease in the Mg/Ca ratio from an initial 5·1 to 3·9, in the Mg/Sr ratio of 0·06 units

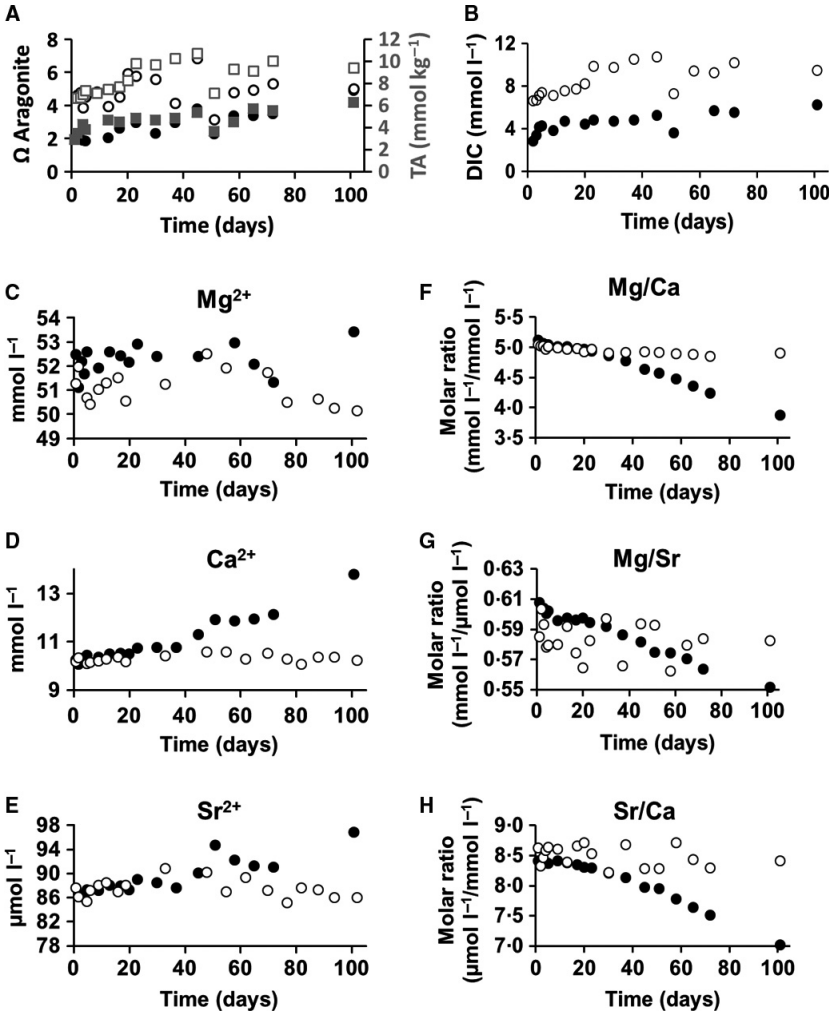

Fig. 4. Medium chemistry of the anoxic sediment incubation: temporal development of (A) $\Omega_{Aragonite}$ (circles) and total alkalinity (TA) (squares); (B) dissolved inorganic carbon (DIC); (C) to (E) divalent cation concentrations; and (F) to (H) divalent cation ratios. Solid symbols show bulk-medium values, and open symbols show control values. Note the variation in the cation control concentrations, apparently caused by errors occurring due to imprecise pipetting of small aliquots.

and in the Sr/Ca ratio from 8·4 to 7·0 (Fig. 4F to H; Table 2).

None of the trends in the *S. sediminis* incubation were observed in the carbonate chemistry of the cell-free control medium, where pH and TA remained stable with values around pH 8 and a TA of 2·3 mmol kg^{-1}, while $\Omega_{Aragonite}$ values fluctuated between 2·7 and 1·7 at the end of the experiment, with a drop to 1·4 on day 51 (Fig. 3A). The DIC increased from an initial 2·4 to 2·7 mmol l^{-1} on day 70 and commuted in ranges of 1·9 and 2·2 mmol l^{-1} towards the end of the experiment (Fig. 3B). The pCO_2 values ranged between 428 μatm and 540 μatm with two peaks on day 20 (616 μatm) and day 37 (717 μatm), and no trend was recognizable in the values throughout the experiment (Table 2). The Ca^{2+}, Mg^{2+} and Sr^{2+} concentrations ranged between 10·4 and 10·1 mmol l^{-1}, 53·1 and 51·2 mmol l^{-1} and 87·5 and 82·5 μmol l^{-1}, respectively (Fig. 3C to E). Consequently, the Mg/Ca ratio was at a constant 5·1 and the Mg/Sr ratio remained stable at 0·6 during the whole experiment, while the Sr/Ca ratio decreased moderately, compared to the sample bearing sediment, from 8·4 to 8·2 (Fig. 3F to H).

The pH in the sediment control slightly decreased with values fluctuating between 7·7 and 7·9 (Table 2). Total alkalinity increased from 6·7 to 12·0 mmol kg^{-1} and $\Omega_{Aragonite}$ increased from an initial value of 3·6 to 6·6 during the experiment (Fig. 4A). The DIC concentration increased from an initial 6·5 to 10·8 mmol l^{-1} at day 70, and decreased to 10·7 mmol l^{-1}, dropped to 7·2 at day 51 and increased to values between 10·1 and 9·0 towards the end of the experiment (Fig. 4B). The pCO_2 values predominantly ranged between 2100 μatm and 3600 μatm, dropped to 1738 and 1675 μatm on days two and three, respectively, and increased to 5957 μatm on day 37 (Table 2). The Ca^{2+} concentrations fluctuated between 10·2, 10·6 and

Table 2. Overview of relevant hydrochemical parameters measured in the frame of this study.

	Ca (mmol l^{-1})	Mg (mmol l^{-1})	Sr (μmol l^{-1})	pH	TA (meq l^{-1})	Ω_{Arag}	DIC (mmol l^{-1})	pCO_2 (μatm)	Ca (mmol l^{-1})	Mg (mmol l^{-1})	Sr (μmol l^{-1})	pH	TA (meq l^{-1})	Ω_{Arag}	DIC (mmol l^{-1})	pCO_2 (μatm)
Bulk seawater									Bulk seawater							
t0 (day 1)	10·08	51·60	85·00	8·06	2·34	2·38	2·44	438·46	10·08	51·60	85·00	8·06	2·34	2·38	2·44	438·46
Shewanella sediminis									Cell-free control							
t0 (day 1)	10·33	53·13	87·51	7·31	1·92	0·3	1·43	1462·96	10·39	53·13	87·51	8·05	2·34	2·4	2·44	449·22
t1 (day 2)	10·28	52·35	85·69	7·54	1·72	0·8	2·64	1608·89	10·22	52·35	85·69	8·26	2·30	(3·9)	2·59	284·38
t2 (day 3)	10·22	52·69	85·79	7·21	2·15	0·1	1·03	1313·69	10·33	52·69	85·79	8·09	2·30	2·7	2·56	427·69
t3 (day 4)	10·21	50·97	83·37	7·18	3·07	0·1	0·86	1171·12	10·07	50·97	83·37	8·06	2·30	2·5	2·54	456·43
t4 (day 5)	10·21	51·69	84·52	7·14	3·14	0·2	1·32	1960·60	10·12	51·69	84·52	8·04	2·30	2·4	2·55	480·96
t5 (day 9)	10·10	51·81	84·71	7·25	4·75	1·1	1·49	1740·62	10·10	51·81	84·71	8·07	2·30	2·5	2·49	436·73
t6 (day 13)	10·41	51·41	84·41	7·38	7·74	1·5	5·08	4445·76	10·10	51·41	84·41	8·04	2·26	2·3	2·48	467·76
t7 (day 16)	10·55	52·41	85·83	7·41	8·55	1·6	6·42	5252·56	10·23	52·41	85·83	8·05	2·30	2·4	2·47	454·74
t8 (day 20)	10·98	53·83	87·27	7·32	9·27	2·0	8·04	8044·55	10·58	53·83	87·27	7·92	2·34	1·9	2·45	616·16
t9 (day 23)	10·67	53·84	87·90	7·46	9·50	4·4	7·71	5635·28	10·58	53·84	87·90	8·08	2·34	2·7	2·53	433·09
t10 (day 31)	11·34	52·50	85·00	7·60	13·34	4·0	11·30	6002·67	10·34	52·50	85·00	8·05	2·26	2·6	2·61	480·51
t11 (day 37)	10·95	N/A	N/A	7·50	15·33	4·5	13·31	8884·99	10·10	N/A	N/A	7·90	2·38	1·9	2·72	717·36
t12 (day 44)	10·96	53·11	86·62	7·48	17·59	5·2	15·86	11078·87	10·48	53·11	86·62	8·02	2·34	2·6	2·74	542·36
t13 (day 51)	10·68	51·85	83·91	7·49	19·93	6·1	18·31	12503·44	10·22	51·85	83·91	7·91	2·34	1·4	1·95	502·21
t14 (day 58)	10·90	51·36	83·66	7·55	20·12	(20·9)	18·13	10799·50	10·12	51·36	83·66	7·93	2·30	N/A	N/A	N/A
t15 (day 65)	10·95	51·57	83·07	8·02	22·99	(19·6)	21·47	N/A	10·16	51·57	83·07	7·96	2·38	N/A	N/A	N/A
t16 (day 72)	10·79	51·24	82·72	7·97	22·80	10·5	22·45	N/A	10·10	51·24	82·72	7·95	2·38	1·7	2·18	510·42
t17 (day 101)	10·49	51·22	82·46	7·70	23·38	10·2	22·45	9466·92	10·11	51·22	82·46	7·97	2·41	1·8	2·18	486·58
Bulk seawater									Bulk seawater							
t0	10·08	51·60	85·00	8·06	2·34	2·38	2·44	438·46	10·08	51·60	85·00	8·06	2·34	2·38	2·44	438·46
Anoxic sediment									Anoxic sediment control							
t0 (day 1)	10·26	52·49	86·37	7·89	2·89	1·9	2·83	764·29	10·16	51·28	87·67	7·83	N/A	5·9	N/A	3111·90
t1 (day 2)	10·07	51·10	84·66	7·85	3·45	2·1	3·41	1012·3	10·34	51·98	86·14	7·90	6·67	4·6	6·59	1738·01
t2 (day 3)	10·31	52·18	86·40	N/A	N/A	N/A	4·20	N/A	10·09	50·67	85·42	7·92	6·76	4·8	6·66	1674·95
t3 (day 4)	10·26	51·68	86·06	7·70	4·26	1·9	4·30	1813·26	10·15	50·41	87·20	7·80	7·05	3·9	7·05	2354·16
t4 (day 5)	10·43	52·58	87·31	7·73	3·80	1·9	3·82	1502·33	10·19	51·02	88·07	7·85	7·37	4·6	7·33	2176·00
t5 (day 9)	10·36	51·92	87·17	7·73	N/A	N/A	N/A	N/A	10·27	51·30	88·44	7·89	7·17	4·9	7·09	1914·76
t6 (day 13)	10·50	52·58	88·01	7·68	4·65	2·1	4·71	2080·43	10·37	51·51	86·99	7·77	7·46	4·0	7·49	2683·17
t7 (day 16)	10·53	52·44	87·92	7·81	4·49	2·6	4·47	1458·00	10·16	50·53	88·02	7·83	7·69	4·5	7·67	2386·83
t8 (day 20)	10·50	52·15	87·29	7·80	N/A	N/A	N/A	N/A	10·42	51·25	90·82	7·91	8·27	5·9	8·17	2104·14
t9 (day 23)	10·73	52·90	88·99	7·82	4·85	3·0	4·83	1538·83	10·56	52·52	90·16	7·81	9·81	5·7	9·82	3203·04
t10 (day 31)	10·77	52·39	88·49	7·72	4·68	2·3	4·72	1899·99	10·58	51·93	86·99	7·80	9·69	5·6	9·71	3242·39
t11 (day 37)	10·77	N/A	87·63	7·82	4·86	3·0	4·84	1542·02	10·28	N/A	89·30	7·65	10·27	4·2	10·47	4956·87
t12 (day 44)	11·31	52·41	90·12	7·87	5·34	3·8	5·29	1497·93	10·52	51·74	87·18	7·85	10·73	6·9	10·69	3173·45

Table 2. (continued)

	Ca (mmol l^{-1})	Mg (mmol l^{-1})	Sr (μmol l^{-1})	pH	TA (meq l^{-1})	Ω_{Arag}	DIC (mmol l^{-1})	pCO_2 (μatm)	Ca (mmol l^{-1})	Mg (mmol l^{-1})	Sr (μmol l^{-1})	pH	TA (meq l^{-1})	Ω_{Arag}	DIC (mmol l^{-1})	pCO_2 (μatm)
t13 (day 51)	11·91	54·45	94·72	7·79	3·63	2·3	3·62	1237·48	10·28	50·49	85·17	7·69	7·15	3·2	7·25	3129·00
t14 (day 58)	11·85	52·97	92·22	7·80	5·59	N/A	N/A	N/A	10·06	50·52	87·60	7·77	9·33	4·8	9·38	3360·23
t15 (day 65)	11·95	52·07	91·30	7·76	5·69	3·4	5·71	2093·88	10·36	50·62	87·35	7·78	9·16	5·0	9·20	3219·52
t16 (day 72)	12·12	51·32	91·09	7·78	5·56	3·5	5·57	1949·21	10·37	50·25	86·07	7·77	10·07	5·3	10·13	3628·90
t17 (day 101)	13·79	53·42	96·81	7·82	6·26	4·9	6·24	1988·06	10·23	50·13	86·07	7·78	9·40	5·0	9·44	3303·51

10·1 mmol l^{-1}, while Mg^{2+} concentrations increased from an initial 51·3 to 52·5 mmol l^{-1} at day 48 and further decreased to a value of 50·1 mmol l^{-1} towards the end of the experiment. The Sr^{2+} concentrations decreased from 87·7 to 86·1 μmol l^{-1} (Fig. 4C to E). The Mg/Ca ratio decreased from 5·1 to 4·9, the Mg/Sr ratio varied around 0·6 and the Sr/Ca ratio decreased from initial 8·6 to 8·4 (Fig. 4F to H; Table 2).

Shell surface structure and bacterial abundance

Stereomicroscopic examination prior to and after incubation displayed partial loss of surface material at areas of shell samples that were exposed to both the *S. sediminis* culture and the anoxic sediment (Fig. 5B and D). Further SEM examination of post-incubation samples revealed stepwise corrosion of surficial shell structures compared to the sample incubated in the cell-free control (Fig. 6). Filtered liquid samples from the shell-cleaning procedure of the *S. sediminis* culture and the anoxic sediment contained dense biofilm fragments, visualized by the DAPI staining (Fig. 7), foremost in the bacterial culture, while the cell-free control liquid did not display any bacterial cells.

Shell elemental composition

Electron microprobe mapping of the shell sample exposed to *S. sediminis* (Fig. 8A), and the sample exposed to the anoxic sediment (Fig. 8B) displayed a decline of Ca content in outer shell parts relative to inner parts and relative to the cell-free control sample (Fig. 8C). The Ca content ranged from 39 wt% of pristine, inner shell parts down to 31 wt% in outer sample parts exposed to the bacterial culture, with the affected area protruding *ca* 90 μm from the outer to the inner sample part. No notable change in Ca content was quantified in the cell-free control sample over the same distance from outer to inner sample area with values of 38 and 39 wt% and no decrease over the distance (Fig. 8C). The sample incubated in the *S. sediminis* culture medium displayed an increase in phosphorous content on the outer surface. However, differences in phosphorous content were at the limit of the analytical resolution. Samples exposed to the cell-free control did not display any change in phosphorous distribution. The EMP mapping of the sample exposed to the anoxic sediment (Fig. 8B) displayed Ca loss on outer surface parts relative to inner parts and

Table 3. $\delta^{13}C$ and $\delta^{18}O$ values of shell samples incubated in the *S. sediminis* culture, anoxic sediment and the cell-free control for sample surfaces. Unaltered samples (no incubation) served as further references.

Sample	Treatment	Comment	$\delta^{13}C_{VPDB}$ [‰]	±s	$\delta^{18}O_{VPDB}$ [‰]	±s
CHA-M-019 AI17 B15	*S. sediminis*	Periostracum	1·49	0·03	4·09	0·06
CHA-M-051 AI32 B1 1	*S. sediminis*	Contact periostracum–mineral	1·81	0·02	2·03	0·11
CHA-M-019 AI17 B1 6	*S. sediminis*	Contact periostracum–mineral	2·19	0·02	2·36	0·08
CHA-M-051 AI32 B1 1	*S. sediminis*	Beneath contact	1·81	0·01	1·74	0·13
CHA-M-019 AI17 B1 6	*S. sediminis*	Beneath contact	2·94	0·04	2·21	0·06
CHA-M-019 AI17 B15	*S. sediminis*	Mineral	1·95	0·02	2·63	0·05
CHA-M-051 AI32 B1 1	*S. sediminis*	Lower side	1·04	0·04	2·66	0·08
CHA-M-019 AI17 B1 6	*S. sediminis*	Lower side	1·59	0·02	2·87	0·05
CHA-M-051 AI32 B1 1	*S. sediminis*	Sawn area	1·20	0·03	2·76	0·09
CHA-M-051 AI32 B1 1	*S. sediminis*	Sawn area	1·24	0·03	2·73	0·09
CHA-M-019 AI17 B1 6	*S. sediminis*	Sawn area	2·77	0·02	2·57	0·11
CHA-M-014-AI12 B4	Anoxic sediment	Periostracum	2·65	0·05	3·69	0·03
CHA-M-012 AI10 B5	Anoxic sediment	Contact periostracum–mineral	2·77	0·02	2·90	0·04
CHA-M-005 AI3 B7	Anoxic sediment	Contact periostracum–mineral	2·44	0·06	2·52	0·09
CHA-M-012 AI10 B5	Anoxic sediment	Beneath contact	3·08	0·04	2·61	0·10
CHA-M-005 AI3 B7	Anoxic sediment	Beneath contact	2·48	0·03	2·30	0·07
CHA-M-014-AI12 B4	Anoxic sediment	Mineral	3·12	0·03	2·57	0·07
CHA-M-012 AI10 B5	Anoxic sediment	Lower side	2·55	0·02	3·69	0·07
CHA-M-005 AI3 B7	Anoxic sediment	Lower side	0·61	0·06	2·71	0·07
CHA-M-012 AI10 B5	Anoxic sediment	Sawn area	2·90	0·05	2·77	0·05
CHA-M-005 AI3 B7	Anoxic sediment	Sawn area	2·04	0·04	2·33	0·06
CHA-M-004 AI2 B1	Cell-free control	Periostracum	−1·03	0·02	0·89	0·07
CHA-M-048 AI29 B1 6	Cell-free control	Contact periostracum–mineral	2·60	0·01	1·85	0·04
CHA-M-048 AI29 B1 6	Cell-free control	Beneath contact	3·14	0·02	2·40	0·10
CHA-M-004 AI2 B1 6	Cell-free control	Mineral	1·88	0·01	1·07	0·03
CHA-M-048 AI29 B1 6	Cell-free control	Lower side	2·81	0·01	4·13	0·07
CHA-M-048 AI29 B1 6	Cell-free control	Sawn area	2·82	0·03	3·40	0·06
CHA-M-048 AI29 B1 12	Unaltered	Contact periostracum–mineral	2·26	0·05	1·95	0·09
CHA-M-048 AI29 B1 13	Unaltered	Beneath contact	2·24	0·04	2·54	0·03
CHA-M-048 AI29 B1 15	Unaltered	Lower side	1·23	0·01	2·27	0·07
CHA-M-048 AI29 B1 14	Unaltered	Sawn area	1·54	0·02	2·51	0·08
CHA-M-048 AI29 B1 20	Unaltered	Contact periostracum–mineral	2·97	0·03	2·73	0·11
CHA-M-048 AI29 B1 21	Unaltered	Beneath contact	3·37	0·02	2·33	0·09
CHA-M-048 AI29 B1 23	Unaltered	Lower side	2·30	0·04	3·07	0·05
CHA-M-048 AI29 B1 22	Unaltered	Sawn area	2·68	0·02	2·56	0·04

the control sample. The Ca content ranged from 38 wt% in inner, pristine shell parts down to 30 wt% in sediment-exposed shell parts, with the affected region protruding >200 μm into the inner regions of the shell sample. The μ-XRF map of the sample exposed to *S. sediminis* (Fig. 9) displayed an increase in the Sr content by 23 ppm in the outer, and by up to 46 ppm in the inner shell parts. The sample exposed to the anoxic sediment revealed an increase in the Sr content by 23 ppm in the outer and 57 ppm in the inner shell parts. Respective areas of the control sample revealed a Sr increase by <11 ppm in the outer shell parts and 80 ppm in the inner shell parts (Fig. 9). Raman spectroscopy prior to and after the experiment displayed the doublet of bands at approximately 701 and 705 cm^{-1} that is typical for aragonite (Fig. 10).

Shell stable carbon and oxygen isotope ratios

Oxygen isotope composition of shell surfaces at and directly beneath the periostracum, and in spatially resolved areas of subsamples exposed to the *S. sediminis* culture displayed a range of 1·7‰ and 4·1‰ whilst carbon isotope composition ranged from 1·0 to 2·9‰. The subsamples exposed to the anoxic sediment displayed a

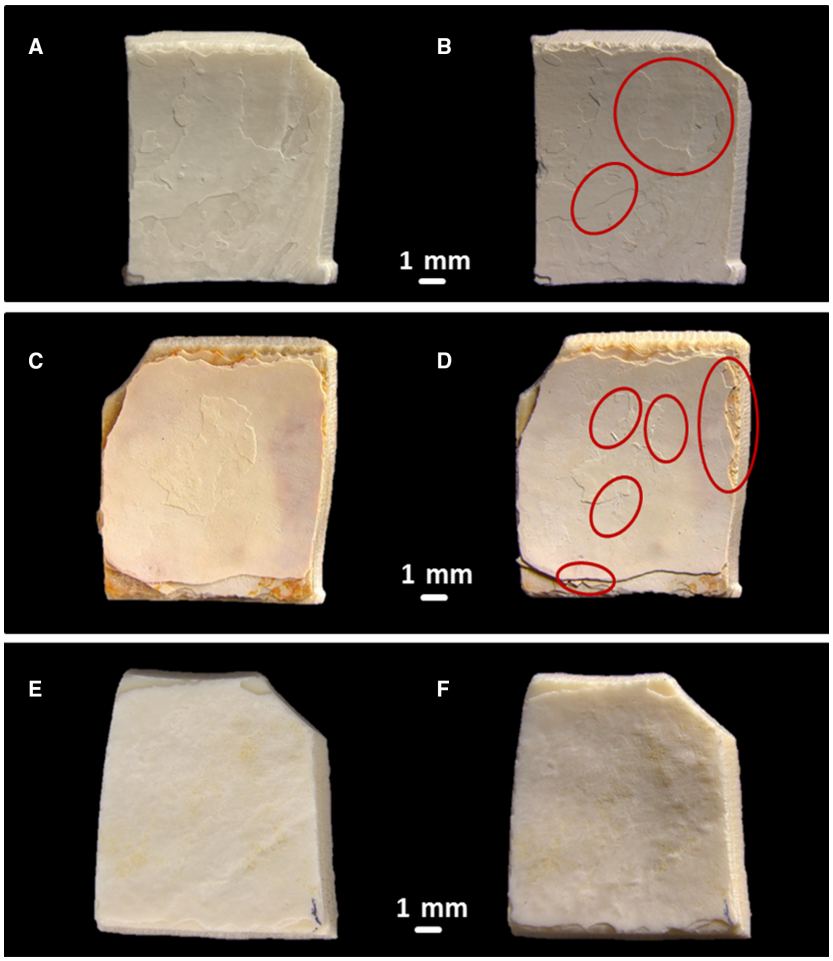

Fig. 5. Stereomicroscopic pictures of shell samples prior to (left) and after incubation (right). Pictures show samples that were incubated in (A) and (B) the bacterial culture; (C) and (D) the anoxic sediment; and (E) and (F) the cell-free control. Red marks display macroscopically visible surface-alteration features. Note that light regimes were not 100% reproducible prior to and after the incubations.

range of 2·3‰ and 3·7‰ in their oxygen isotope composition, and carbon ranged from 0·6 to 3·1‰ (Table 3; Fig. 11). Oxygen isotope composition of subsamples from the cell-free control ranged from 0·9 to 4·1‰ and carbon isotope composition from −1·0 to 3·1‰, while unaltered reference samples displayed a spatial variability of 1·9 to 2·5‰ and 2·3 to 3·1‰ in oxygen isotopic composition, and carbon ranged from 1·2 to 2·3‰ and 2·3 to 3·4‰.

Liquid medium samples were not analysed; however, it is expected that both carbon and oxygen isotopes in the minute volumes of aragonite that dissolved from the shell or exchanged with the experimental fluid were too small to affect the bulk water or sediment isotope ratios.

INTERPRETATION AND DISCUSSION

Despite the extremely short experimental duration of three months in comparison with geological timescales available for diagenesis, noteworthy alterations were detected in the carbonate chemistry of the liquid phase of both the *S. sediminis* culture and the anoxic sediment. These were echoed by alterations of the surficial shell ultrastructure and the elemental composition of the shell. Implications of these findings will be discussed in more detail in the following sections.

Microbial alteration of the aragonitic structure and geochemistry of the shell

Alteration at the species level: Shewanella sediminis

Shewanella sediminis is capable of hydrolysing chitin polymers by means of a chitinase, and of subsequent oxidation and fermentation of the chitin monomer unit N-acetylglucosamine (Yang *et al.*, 2006; Rodionov *et al.*, 2010). Chitin is one of the main structural constituents of the mollusc organic matrix, from which aragonite biomineral nucleation, growth and architecture

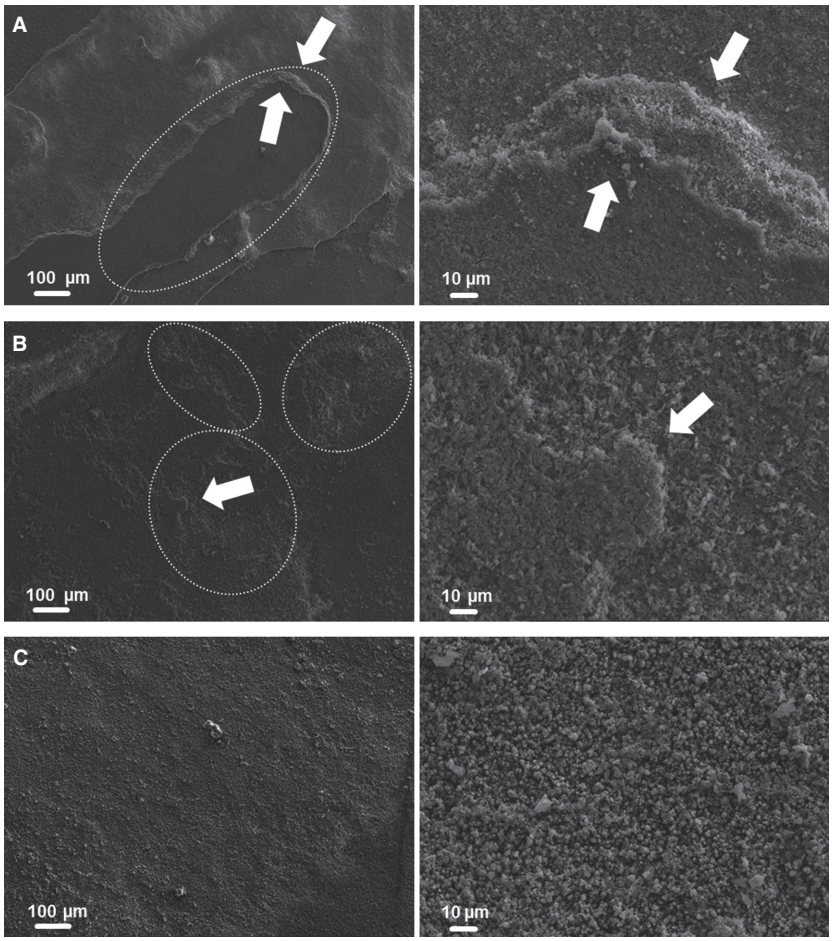

Fig. 6. Scanning electron microscopy (SEM) pictures of shell samples incubated in (A) the *S. sediminis* culture; (B) the anoxic sediment; and (C) the cell-free control. Dotted circles indicate altered areas, and arrows indicate surface dissolution features. Check for scales.

are controlled (Lowenstam & Weiner, 1989; Weiner & Addadi, 2011). The degradation of the resulting intracrystalline and intercrystalline organic framework (Marin *et al.*, 1996) consequently increases the reactive surface for entering pore water (medium) fluid as well as bacterial cells and EPS, and with it potentially enhancing the effects of alteration processes. The suggested underlying mechanisms for aragonite dissolution in the *S. sediminis* culture incubation include the hydrolysis of chitin polymers by *S. sediminis* chitinase, followed by fermentation of N-acetylglucosamine during cell attachment to the mineral and subsequent shell surface dissolution through acidic fermentation products.

Results of stereomicroscopic and SEM analyses displayed structural dissolution features, and are further supplemented by the loss of Ca detected by shell sample EMP mapping as well as the increased Ca^{2+} concentrations in the *S. sediminis* culture medium. Yet Sr^{2+} concentrations in the medium decreased over time although, expectedly, values should have increased due to aragonite dissolution. This intuitively contradictory outcome can be explained through the effect of divalent cation scavenging by bacterial biofilm EPS (McCalla, 1939). Because biofilm fragments were isolated from incubated shell samples, the presence of related EPS is expected. Adsorption of divalent cations occurs via electrostatic binding sites within the EPS, with the charge of functional groups allowing for binding of the cations as a function of pH (Liu & Fang, 2002; Comte *et al.*, 2008). The reported pK_a values range from 4·8 for carboxyl up to 11 for hydroxyl groups. A study by Guibaud *et al.* (2008) additionally suggested EPS-binding affinity to be cation species specific. The hydration enthalpy differs among Mg, Ca and Sr ions, with the latter showing the lowest value of $-1444{\cdot}7$ $-\Delta H$ kJ mol^{-1} (Burgess, 1978). Given the decreasing Sr^{2+} concentration in the medium over time, preferred binding of Sr^{2+} to EPS functional groups, relative to Ca^{2+} or Mg^{2+}, is feasible and could account for the

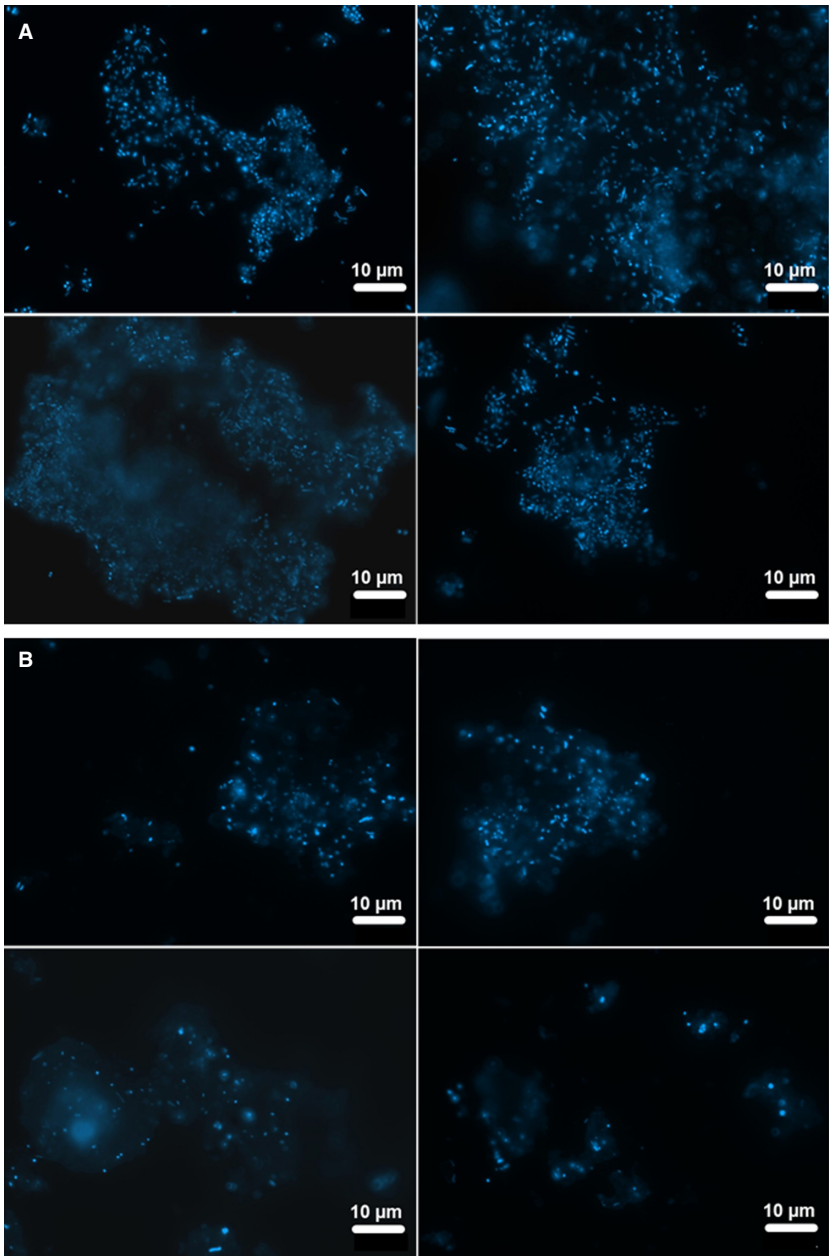

Fig. 7. Stereomicroscopic pictures of biofilm fragments isolated from the cleaning procedure of: (A) the *S. sediminis* culture; and (B) the anoxic sediment. Cells were stained with 4,6 diamidino-2-phenylindole (DAPI).

enrichment of Sr^{2+} on the sample margins detected by the μ-XRF mapping. Exchange of lost shell Ca^{2+} with pore fluid Sr^{2+} from enriched bacterial EPS could have fostered this enrichment. However, no high-resolution analyses of the biofilms are at hand to underpin this hypothesis, and the high Sr^{2+} content at the control inner shell rim suggests a generally higher Sr content in that region.

Furthermore, the cell wall of *Shewanella* sp. has a high adsorption affinity for dissolved Sr^{2+} with a maximum sorptive capacity of reactive surfaces for Sr^{2+} of 0·075 (*Shewanella alga*) and 0·079 mmol·g^{-1} (*Shewanella putrefaciens*) when cells are coated with Fe(III) oxide (Small *et al.*, 1999). Whilst in this study the addition of Fe (III) to the *S. sediminis* culture medium could have facilitated a cell wall–cation interaction similar to the observations by Small *et al.* (1999), the described Sr^{2+} scavenging abilities are a function of pH and the process requires protonated functional groups at low pH (5·5 to 5·9) that serve as Sr^{2+} binding sites. However, given that the pH in bacterial EPS can differ substantially from that of the surrounding environment (Hunter & Beveridge, 2005), Sr^{2+}

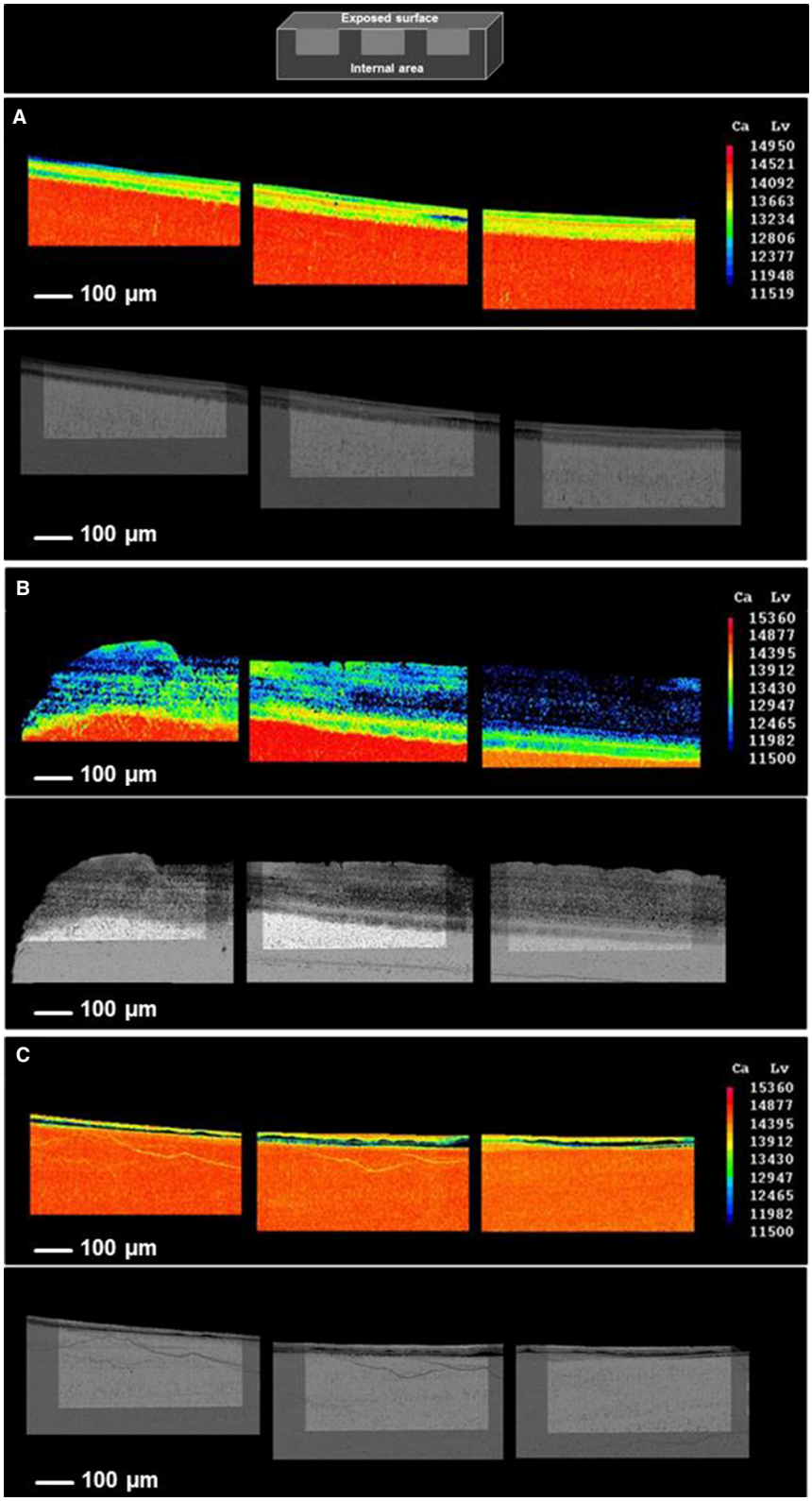

Fig. 8. Electron microprobe maps of shell samples incubated in: (A) the *S. sediminis* culture; (B) the anoxic sediment; and (C) the cell-free control (note fissure in the control sample leading to rim artefacts that resemble loss in Ca). Samples were sawn perpendicular, the upper sample parts are the surfaces exposed to the incubations, and the lower parts are the inner, pristine sample area. Maps show intensity in counts per second. Backscattered electron microscopy (BSE) pictures display the measured areas within the samples.

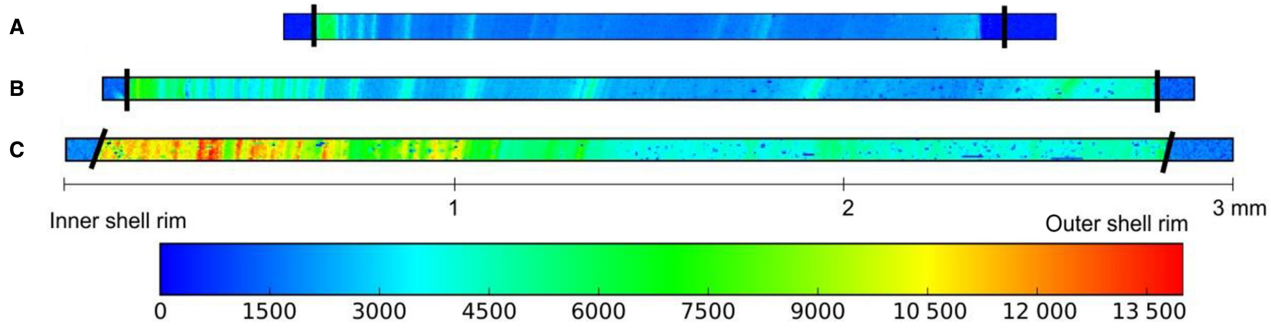

Fig. 9. μ-XRF maps of Sr L-edge along the transects of *A. islandica* shells incubated in (A) the *S. sediminis* culture; (B) the cell-free control; and (C) the anoxic sediment. Concentrations are displayed in counts per second. The marked left and right parts of the maps display the resin in which the samples were embedded. In sample (A), the periostracum is still present and is characterized by an absence of strontium.

adsorption within the *S. sediminis* EPS is feasible despite the comparably high pH in the *S. sediminis* medium. Adsorption of divalent cations could also account for the observed Mg^{2+} decrease in the medium. The simultaneously observed increase in Ca^{2+} concentrations presumably results from the observed loss of Ca in the shell, and Ca^{2+} adsorption is consequently reflected by the subsequent decrease in Ca^{2+} medium concentration. Moreover, cation complexation by bacterial EPS, here specifically EPS functional groups, could explain why, despite the strong increase in TA and $\Omega_{Aragonite}$, no inorganic carbonate precipitation took place within the medium according to microscopic observations.

The undersaturation of the *S. sediminis* incubation medium with respect to aragonite at the experimental start (Fig. 3) remains unresolved, because solely the inoculated bacterial culture could have had an effect on medium $\Omega_{Aragonite}$, but the undersaturation remained for five days.

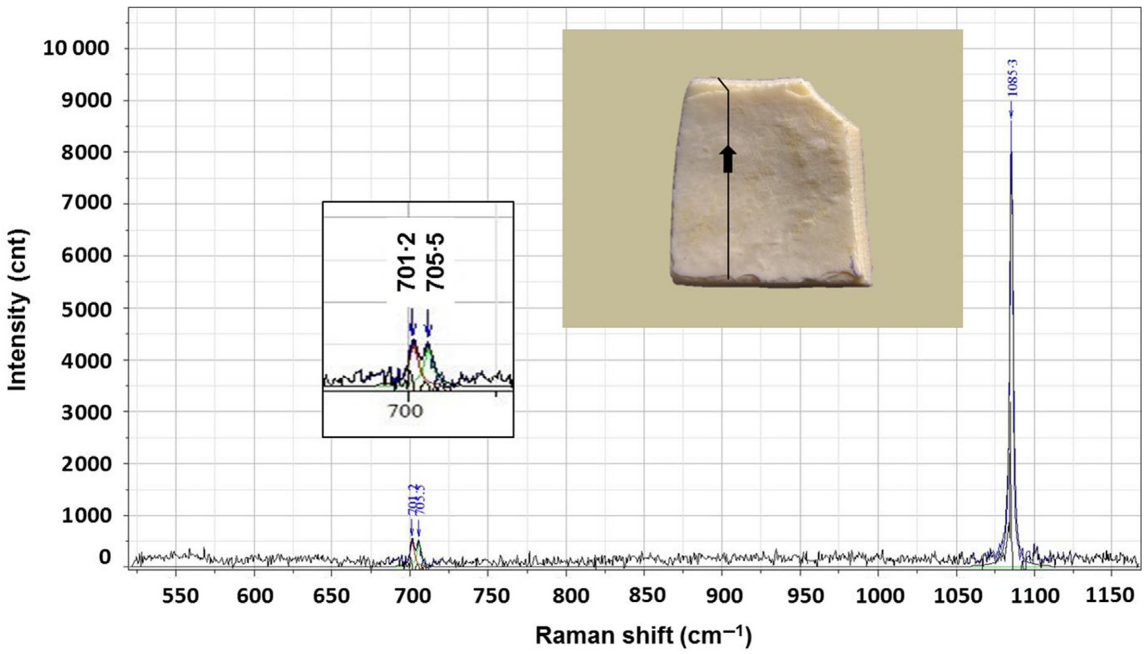

Fig. 10. Example of output from a Raman spectroscopic scan conducted on an *A. islandica* shell sample after incubation in the bacterial culture medium (the conducted transect is indicated on the sample picture). The doublet displays the bending mode v4 of the carbonate ion in aragonite.

Furthermore, Ca^{2+} concentrations did not reflect the low $\Omega_{Aragonite}$ of the medium. The onset of bacterial fermentation is depicted in the slight pH decrease that is correlated with an increase in TA. The increasing Ca^{2+} concentrations in the medium indicate subsequent shell dissolution, caused by fermentation products, and Ca^{2+} values furthermore suggest a ceasing dissolution process from day 37 on. However, pH and TA increased beyond this point of time, and the pCO_2 reached a peak value of 12 500 μatm (Table 2). It is therefore apparent that pH and TA in the medium were dominated by CO_2 degassing into the headspace during pivoting of the beakers. Furthermore, sample equilibration with the atmosphere during the sampling procedure and pH measurements led to a substantial change in the pCO_2 values.

Alteration at the community level: anoxic sediment

The microbial biota in marine sediments accounts for diverse metabolic processes (Jørgensen, 2006; Orcutt *et al.*, 2011) that, via the generation of alkaline or acidic metabolites, facilitate either carbonate precipitation or dissolution, respectively. During earliest burial into sediments, biogenic carbonates are exposed to anaerobic bacterial communities such as denitrifiers, Mn-reducing, Fe-reducing and sulphate-reducing bacteria. Respective respiratory processes account for an alkalinity increase in the environment through generation of HCO_3^-; this in turn facilitates authigenic carbonate nucleation and precipitation (Berner *et al.*, 1970; Castanier *et al.*, 1999; Van Lith *et al.*, 2003). Closed-system model calculations suggest that sulphate reduction does not induce carbonate precipitation but, on the contrary, leads to a drop in both pH and saturation index (SI) due to generation of one mole H^+ per mole sulphur turnover (Meister, 2013). In contrast, experimental approaches have demonstrated that sulphate-reducing bacteria in particular can have an enhanced effect on environmental alkalinity, pH and SI, for example, through the usage of metabolic hydrogen (H_2) and formate produced by bacterial fermentation (Gallagher *et al.*, 2014). At present, both statements are controversially discussed. The sulphate reduction zone is vertically followed by the methanogenic zone, where CO_2 is withdrawn from the system via archaea-driven methanogenesis (Nealson, 1997; Jørgensen, 2006) implying a further increase in pH. Overall, the majority of anaerobic microbial metabolic processes account for an increase in system alkalinity and pH that

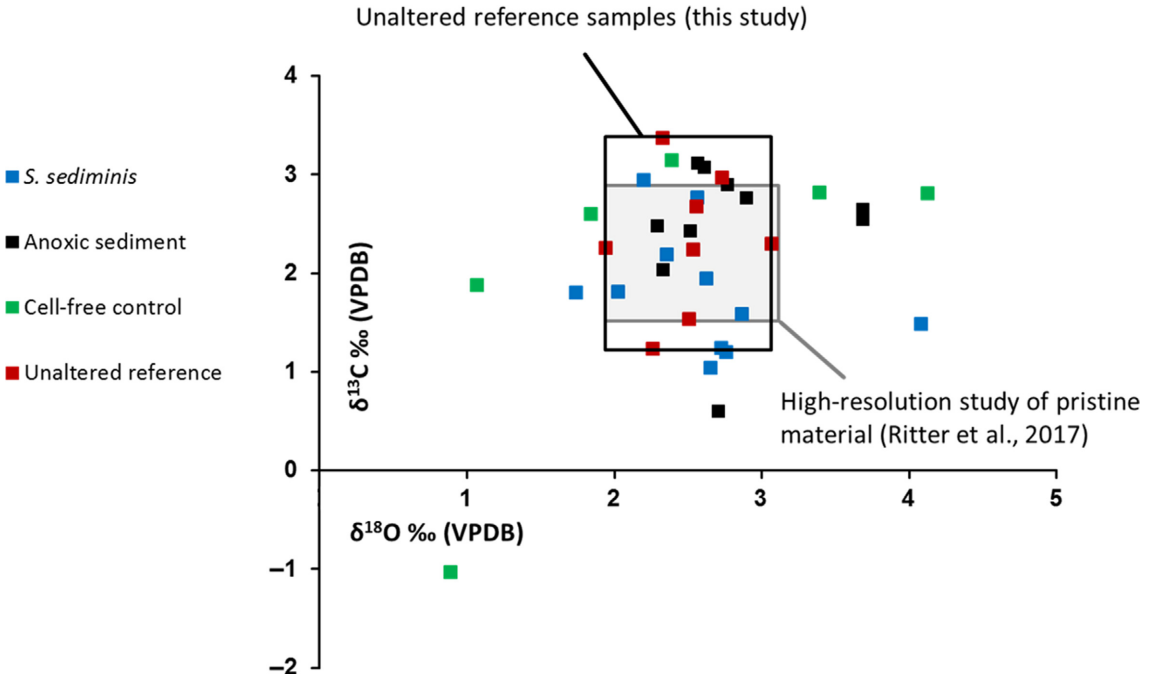

Fig. 11. $\delta^{13}C$ and $\delta^{18}O$ values for sample surfaces of shell samples incubated in the *S. sediminis* culture, the anoxic sediment, the cell-free control and unaltered reference samples.

has the potential to facilitate carbonate precipitation in marine sediments. While the anoxic sediment medium of this study displayed distinct increases in TA and $\Omega_{Aragonite}$ over time as would be expected from anaerobic microbial organic matter degradation, the increasing CO_2 partial pressure followed by stabilization, medium divalent cation concentrations (Fig. 4C to E) and shell sample constitution (Figs 5, 6 and 8) indicated that rather carbonate dissolution caused these increases. The increase in Sr^{2+} concentrations in the incubation medium resulted in a decreasing Mg/Sr ratio. A comparably stronger increase in Ca^{2+} concentrations was consequently reflected by a distinct decrease in Mg/Ca and Sr/Ca ratios. In contrast, the anoxic sediment control underwent an increase in TA and pCO_2 along with a minor decrease in pH, reflecting heterotrophic benthic activity, and no clear trend was displayed in the control divalent cation concentrations.

Cell aggregations isolated from the incubated shell samples confirmed the attachment of bacterial biofilms to the shell surface, stereomicroscopic examinations of the shell outer surface indicated exfoliation, while SEM pictures displayed a stepwise retreating surface structure that was indicative of dissolution of the surficial structure. No evidence for a newly formed carbonate phase was found on these surfaces. Additionally, Raman spectroscopy of the sample provided no indication of carbonate polymorphs other than aragonite, thus excluding microbially induced non-stoichiometric dolomite or high-Mg calcite precipitation. Electron microprobe mapping revealed Ca loss on the sample part exposed to the sediment. The EMP intensity maps displayed a decrease in Ca^{2+} concentration towards the shell surface over a depth of >200 μm. This decrease in Ca^{2+} supports the observed structural changes, as well as the increase in $\Omega_{Aragonite}$, and indicates a slow, continuous dissolution process. Data from the sediment control medium displayed strong variations in all measured medium parameters and an increase in carbonate system parameters over time, the latter reflecting anoxic sediment habitats dominated by bicarbonate-generating anaerobic metabolic processes. However, the distinct increase in Ca^{2+} and Sr^{2+} concentration over time determined in the anoxic sediment incubation was not reflected in the sediment control data.

All sediment samples were taken in the midst of April, when spring bloom in the North Sea was supposedly just developing (Wiltshire *et al.*, 2008) and subsequent sedimentation of organic carbon had probably not reached the sea floor (water depth at sampling station = 17 m). It is therefore plausible that due to the lack of available labile organic carbon in the sediment, constituents of the shell periostracal, intercrystalline and intracrystalline organic matter were used as metabolic substrates by a variety of bacteria. The subsequent increase in reactive surface area would have supported dissolution processes, which in turn resulted in the addition of Ca and Sr ions into the anoxic medium. Metal ion complexation on the charge of bacterial cell walls is a function of pH (Konhauser & Riding, 2012). The increasing pH in the medium, resulting from carbonate dissolution and anaerobic organic matter degradation, might have led to an increasing net negative charge of cell wall surface and/or EPS functional groups. Both effects would consequently lead to a high affinity for binding of the metal cations; this could furthermore explain the increase in Sr^{2+} counts in the outer sample margins that was detected via μ-XRF mapping and presumably reflects direct microbe–mineral interaction in that area.

Alteration of carbon and oxygen isotope data

Isotope data ($\delta^{13}C$ and $\delta^{18}O$) measured from shell subsamples exposed to incubation experiments were compared against the natural variability of carbon and oxygen isotope ratios in *A. islandica* bivalves. Previously reported $\delta^{13}C$ values for *A. islandica* shells from different origins range between $-0{\cdot}7‰$ (Butler *et al.*, 2009) and $+4{\cdot}0‰$ (Schöne, 2005), and $\delta^{18}O$ values between $-1{\cdot}7‰$ (Dunca *et al.*, 2009) and $+3{\cdot}6‰$ (Schöne *et al.*, 2004). High-resolution analyses by Ritter *et al.* (2017) documented a primary spatial variability of $\pm4{\cdot}2‰$ for $\delta^{13}C$ and of $\pm1{\cdot}1‰$ for $\delta^{18}O$ in replicate shell samples from the bulk material used for this experiment. Consequently, unaltered *A. islandica* shells exhibit a substantial intershell and intrashell isotopic variability that introduces a significant level of complexity in the comparison of pre-incubation and post-incubation isotope geochemistry of the shells. Moreover, the mere sawing or drilling of aragonite, or even the removal of material from the surface with a scalpel, may induce a partial neomorphic change to calcite. Neomorphism in turn affects both carbon and oxygen isotope ratios depending on the percental transition from aragonite to calcite (Staudigel & Swart, 2016). All of these issues suggest that care should be taken with the interpretation of the presented data set.

In essence, shell subsamples from the *S. Sediminis* and the anoxic sediment experiments displayed an increased scatter for both $\delta^{13}C$ and $\delta^{18}O$ relative to high-resolution micro-milled samples from pristine shells (Ritter *et al.*, 2017). Clearly, the range in $\delta^{13}C$ (>4‰) is more pronounced relative to $\delta^{18}O$. Remarkably, however, the most ^{18}O-enriched sample originates from a cell-free control experiment. Finally, when comparing isotope data from different incubation experiments and different sampling sites, no obvious trend emerges (Fig. 11).

In conclusion, this study shows that the present data are potentially interesting and relevant, particularly in the light of previous work suggesting an impact of microbe metabolism on carbonate isotope ratios (Londry & Des Marais, 2003). At present, however, it seems unclear to which degree the choice of: (i) a specific sampling site within a subsample (i.e. outer shell, inner shell, surface and centre); (ii) the sampling bias resulting in aragonite–calcite neomorphism; and (iii) the primary seasonal variability in aragonite isotope geochemistry must be placed against genuine bacteria-induced patterns. The way forward must lie in significantly expanded experimental duration (more than 12 months) and a very detailed and careful sampling strategy of comparable material from comparable shell subsamples.

CONCLUSIONS

The present study identifies the potential of marine benthic bacteria to affect ultrastructural and geochemical properties of *Arctica islandica* shells over an experimental time span of three months. Processes observed included the partial dissolution of the surficial shell crystal ultrastructure and the alteration of the biomineral's geochemical and (to a less indicative degree) isotopic composition. It is hypothesized in this study that the disintegration of intercrystalline organic matter opened pathways for reactive fluids to enter the carbonate hard parts, leading to enhanced rates of fluid–carbonate interaction. Additionally, it is suggested that microbially induced aragonite alteration could play a so far underappreciated role in sea floor and earliest burial diagenetic realms. These alteration processes have – over geological timescales – the potential to compromise aragonitic proxy archives. Long-term incubations (of more than 12 months) in future studies could help to decipher these potential diagenetic effects.

ACKNOWLEDGEMENTS

We thank captain and crew of the *R/V Heincke* and *RC Suedfall*, T. Wilkop and K. Ricklefs for provision of seawater and the opportunity for sediment sampling, respectively. We thank D. Buhl for shell preparation, F. Melzner and M. Haeckel for provision of microscopy and Raman facilities, respectively, and A. Dale for his input on equilibration processes. We thank B. Domeyer and R. Surberg for geochemical analyses, and N. Bigalke and M. Thöner for technical support. Additional thanks go to G. Schuessler and P. Wefers of the AG Geobiology for their laboratory assistance. This study was conducted within the Forschergruppe 1644 CHARON funded by the German Research Foundation (DFG). We thank Chief Editor Della Porta and three reviewers for their valuable comments.

REFERENCES

Abele, D., **Strahl, J.**, **Brey, T.** and **Philipp, E.E.R.** (2008) Imperceptible senescence: ageing in the ocean quahog *Arctica islandica*. *Free Radical Res.*, **42**, 474–480.

Aloisi, G., **Gloter, A.**, **Krüger, M.**, **Wallmann, K.**, **Guyot, F.** and **Zuddas, P.** (2006) Nucleation of calcium carbonate on bacterial nanoglobules. *Geology*, **34**, 2017–2020.

Bathurst, R.G.C. (1975) *Carbonate Sediments and Their Diagenesis (Developments in Sedimentology)*. Elsevier Science, Oxford, 640 pp.

Berner, R.A. (1980) *Early Diagenesis: A Theoretical Approach*. Princeton University Press, New Jersey, 256 pp.

Berner, R.A., **Scott, M.R.** and **Thomlinson, C.** (1970) Carbonate alkalinity in the pore waters of anoxic marine sediments. *Limnol. Oceanogr.*, **15**, 544–549.

Beveridge, T.J. and **Murray, R.G.** (1980) Sites of metal deposition in the cell wall of *Bacillus subtilis*. *J. Bacteriol.*, **141**, 876–887.

Braissant, O., **Decho, A.W.**, **Dupraz, C.**, **Glunk, C.**, **Przekop, K.M.** and **Visscher, P.T.** (2007) Exopolymeric substances of sulfate-reducing bacteria: interactions with calcium at alkaline pH and implication for formation of carbonate minerals. *Geobiology*, **5**, 401–411.

Burgess, J. (1978) *Metal Ions in Solution*. Halsted Press, New York, 481 pp.

Butler, P.G., **Scourse, J.D.**, **Richardson, C.A.**, **Wanamaker, A.**, **Bryant, C.L.** and **Bennell, J.D.** (2009) Continuous marine radiocarbon reservoir calibration and the 13 C Suess effect in the Irish Sea: results from the first multicentennial shell-based marine master chronology. *Earth Planet. Sci. Lett.*, **279**, 230–241.

Butler, P.G., **Wanamaker, A.D.**, **Scourse, J.D.**, **Richardson, C.A.** and **Reynolds, D.J.** (2013) Variability of marine climate on the North Icelandic Shelf in a 1357-year proxy archive based on growth increments in the bivalve *Arctica islandica*. *Palaeogeogr. Palaeoclimatol. Palaeoecol.*, **373**, 141–151.

Cai, W.-J., **Chen, F.**, **Powell, E.N.**, **Walker, S.E.**, **Parsons-Hubbard, K.M.**, **Staff, G.M.**, **Wang, Y.**, **Ashton-Alcox, K.A.**, **Callender, W.R.** and **Brett, C.E.** (2006) Preferential

dissolution of carbonate shells driven by petroleum seep activity in the Gulf of Mexico. *Earth Planet. Sci. Lett.*, **248**, 227–243.

Castanier, S., **Le Métayer-Levrel, G.** and **Perthuisot, J.-P.** (1999) Ca-carbonates precipitation and limestone genesis – the microbiogeologist point of view. *Sed. Geol.*, **126**, 9–23.

Chafetz, H.S. and **Buczynski, C.** (1992) Bacterially induced lithification of microbial mats. *Palaios*, **7**, 277–293.

Comte, S., **Guibaud, G.** and **Baudu, M.** (2008) Biosorption properties of extracellular polymeric substances (EPS) towards Cd, Cu and Pb for different pH values. *J. Hazard. Mater.*, **151**, 185–193.

Coughlin, R.T., **Tonsager, S.** and **McGroarty, E.J.** (1983) Quantitation of metal cations bound to membranes and extracted lipopolysaccharide of *Escherichia coli*. *Biochemistry*, **22**, 2002–2007.

Davis, K.J., **Nealson, K.H.** and **Lüttge, A.** (2007) Calcite and dolomite dissolution rates in the context of microbe-mineral surface interactions. *Geobiology*, **5**, 191–205.

Decho, A.W. (2010) Overview of biopolymer-induced mineralization: what goes on in biofilms? *Ecol. Eng.*, **36**, 137–144.

Decho, A.W., **Visscher, P.T.** and **Reid, R.P.** (2005) Production and cycling of natural microbial exopolymers (EPS) within a marine stromatolite. *Palaeogeogr. Palaeoclimatol. Palaeoecol.*, **219**, 71–86.

Dodd, J. (1963) Paleoecological implications of shell mineralogy in two pelecypod species. *J. Geol.*, **71**, 1–11.

Dunca, E., **Mutvei, H.**, **Göransson, P.**, **Mörth, C.M.**, **Schöne, B.R.**, **Whitehouse, M.J.**, **Elfman, M.** and **Baden, S.P.** (2009) Using ocean quahog (*Arctica islandica*) shells to reconstruct paleoenvironment in Öresund, Kattegat and Skagerrak, Sweden. *Int. J. Earth Sci.*, **98**, 3–17.

Dupraz, C., **Visscher, P.T.**, **Baumgartner, L.K.** and **Reid, R.P.** (2004) Microbe-mineral interactions: early carbonate precipitation in a hypersaline lake (Eleuthera Island, Bahamas). *Sedimentology*, **51**, 745–765.

Froelich, P.N., **Klinkhammer, G.P.**, **Bender, M.L.**, **Luedtke, N.A.**, **Heath, G.R.**, **Cullen, D.**, **Dauphin, P.**, **Hammond, D.** and **Hartman, B.** (1979) Early oxidation of organic matter in pelagic sediments of the eastern equatorial Atlantic: suboxic diagenesis. *Geochim. Cosmochim. Acta*, **43**, 1057–1090.

Gallagher, K., **Dupraz, C.** and **Visscher, P.** (2014) Two opposing effects of sulfate reduction on carbonate precipitation in normal marine, hypersaline, and alkaline environments: comment. *Geology*, **42**, e313–e314.

Greenfield, L. (1962) Metabolism and concentration of calcium and magnesium and precipitation of calcium carbonate by a marine bacterium. *Ann. N. Y. Acad. Sci.*, **109**, 23–45.

Guibaud, G., **Bordas, F.**, **Saaid, A.**, **D'Abzac, P.** and **Van Hullebusch, E.** (2008) Effect of pH on cadmium and lead binding by extracellular polymeric substances (EPS) extracted from environmental bacterial strains. *Colloids Surf. B*, **63**, 48–54.

Hillgärtner, H., **Dupraz, C.** and **Hug, W.** (2001) Microbially induced cementation of carbonate sands: are micritic meniscus cements good indicators of vadose diagenesis? *Sedimentology*, **48**, 117–131.

Himmler, T., **Brinkmann, F.** and **Bohrmann, G.** (2011) Corrosion patterns of seep-carbonates from the eastern Mediterranean Sea. *Terra Nova*, **23**, 206–212.

Hunter, R.C. and **Beveridge, T.J.** (2005) Application of a pH-sensitive fluoroprobe (C-SNARF-4) for pH microenvironment analysis in *Pseudomonas aeruginosa* biofilms. *Appl. Environ. Microbiol.*, **71**, 2501–2510.

Immenhauser, A., **Schöne, B.R.**, **Hoffmann, R.** and **Niedermayr, A.** (2016) Mollusc and brachiopod skeletal hard parts: intricate archives of their marine environment. *Sedimentology*, **63**, 1–59.

Jørgensen, B.B. (2006) Bacteria and marine biogeochemistry. In: *Marine Geochemistry* (Eds H.D. Schulz and M. Zabel), pp. 173–207. Springer, Berlin, Heidelberg.

Kawaguchi, T. and **Decho, A.W.** (2002) A laboratory investigation of cyanobacterial extracellular polymeric secretions (EPS) in influencing $CaCO_3$ polymorphism. *J. Cryst. Growth*, **240**, 230–235.

Konhauser, K. and **Riding, R.** (2012) Bacterial biomineralization. In: *Fundamentals of Geobiology* (Eds A. Knoll, D. Canfield and K. Konhauser), pp. 105–130. Blackwell Science, Oxford.

Konhauser, K.O., **Fyfe, W.S.**, **Ferris, F.G.** and **Beveridge, T.J.** (1993) Metal sorption and mineral precipitation by bacteria in two Amazonian river systems: Rio Solimoes and Rio Negro, Brazil. *Geology*, **21**, 1103–1106.

Krause, S., **Aloisi, G.**, **Engel, A.**, **Liebetrau, V.** and **Treude, T.** (2014) Enhanced calcite dissolution in the presence of the aerobic methanotroph *Methylosinus trichosporium*. *Geomicrobiol J.*, **31**, 325–337.

Little-Gadow, S. (1982) Sediment und Gefüge. In: *Das Watt; Ablagerungs-und Lebensraum* (Ed. H.E. Reineck), pp. 51–62. Waldemar Kramer, Frankfurt a.M.

Liu, H. and **Fang, H.H.P.** (2002) Characterization of electrostatic binding sites of extracellular polymers by linear programming analysis of titration data. *Biotechnol. Bioeng.*, **80**, 806–811.

Londry, K.L. and **Des Marais, D.J.** (2003) Stable carbon isotope fractionation by sulfate-reducing bacteria. *Appl. Environ. Microbiol.*, **69**, 2942–2949.

Lowenstam, H.A. and **Weiner, S.** (1989) *On Biomineralization*. Oxford University Press, Oxford, 324 pp.

Lüttge, A., **Zhang, L.** and **Nealson, K.H.** (2005) Mineral surfaces and their implications for microbial attachment: results from Monte Carlo simulations and direct surface observations. *Am. J. Sci.*, **305**, 766–790.

Marin, F. (2012) The formation and mineralization of mollusk shell. *Front Biosci.*, **S4**, 1099–1125.

Marin, F., **Smith, M.**, **Isa, Y.**, **Muyzer, G.**, **Westbroek, P.**, **Isat, Y.**, **Muyzert, G.** and **Westbroek, P.** (1996) Skeletal matrices, muci, and the origin of invertebrate calcification. *Proc. Natl Acad. Sci. USA*, **93**, 1554–1559.

McCalla, T.M. (1939) Cation adsorption by bacteria. *J. Bacteriol.*, **40**, 23–32.

Meister, P. (2013) Two opposing effects of sulfate reduction on carbonate precipitation in normal marine, hypersaline, and alkaline environments. *Geology*, **41**, 499–502.

Nealson, K.H. (1997) Sediment bacteria: who's there, what are they doing, and what's new? *Annu. Rev. Earth Planet. Sci.*, **25**, 403–434.

Orcutt, B.N., **Sylvan, J.B.**, **Knab, N.J.** and **Edwards, K.J.** (2011) Microbial Ecology of the Dark Ocean above, at, and below the Seafloor. *Microbiol. Mol. Biol. Rev.*, **75**, 361–422.

Paine, S.G., **Linggood, F.V.**, **Schimmer, F.** and **Thrupp, T.C.** (1933) The relationship of micro-organisms to the decay of stone. *Phil. Trans. Roy. Soc. London B Biol. Sci.*, **222**, 97–127.

Pavlova, GYu, **Tishchenko, P.Ya**, **Volkova, T.I.**, **Dickson, A.** and **Wallmann, K.** (2008) Intercalibration of Bruevich's

method to determine the total alkalinity in seawater. *Oceanology*, **48**, 438–443.

Pratje, O. (1932) Die Sedimente der Deutschen Bucht. Wissenschaftl. Meeresuntersuch., Abt. Helgoland, N. F. 18, **6**.

Riding, R. (2000) Microbial carbonates: the geological record of calcified bacterial algal mats and biofilms. *Sedimentology*, **47**, 179–214.

Ritter, A.-C., **Mavromatis, V.**, **Dietzel, M.**, **Kwiecien, O.**, **Wiethoff, F.**, **Griesshaber, E.**, **Casella, L.A.**, **Schmahl, W.W.**, **Koelen, J.**, **Neuser, R.**, **Leis, A.**, **Buhl, D.**, **Niedermayr, A.**, **Breitenbach, S.F.M.**, **Bernasconi, S.M.** and **Immenhauser, A.** (2017) Exploring the impact of diagenesis on (isotope) geochemical and microstructural alteration features in biogenic aragonite. *Sedimentology*, **64**, 1354–1380. https://doi.org/10.1111/sed.12356.

Rodionov, D.A., **Yang, C.**, **Li, X.**, **Rodionova, I.A.**, **Wang, Y.**, **Obraztsova, A.Y.**, **Zagnitko, O.P.**, **Overbeek, R.**, **Romine, M.F.**, **Reed, S.**, **Fredrickson, J.K.**, **Nealson, K.H.** and **Osterman, A.L.** (2010) Genomic encyclopedia of sugar utilization pathways in the *Shewanella* genus. *BMC Genom.*, **11**, 494.

Sánchez-Román, M., **Rivadeneyra, M.A.**, **Vasconcelos, C.** and **McKenzie, J.A.** (2007) Biomineralization of carbonate and phosphate by moderately halophilic bacteria. *FEMS Microbiol. Ecol.*, **61**, 273–284.

Schindler, M. and **Osborn, M.J.** (1979) Interaction of divalent cations and polymyxin B with lipopolysaccharide. *Biochemistry*, **18**, 4425–4430.

Schöne, B.R. (2005) Daily growth rates in shells of *Arctica islandica*: assessing sub-seasonal environmental controls on a long-lived bivalve mollusk. *Palaios*, **20**, 78–92.

Schöne, B.R. (2013) *Arctica islandica* (Bivalvia): a unique paleoenvironmental archive of the northern North Atlantic Ocean. *Global Planet. Change*, **111**, 199–225.

Schöne, B.R., **Castro, A.**, **Fiebig, J.** and **Houk, S.D.** (2004) Sea surface water temperatures over the period 1884–1983 reconstructed from oxygen isotope ratios of a bivalve mollusk. *Palaeogeogr. Palaeoclimatol. Palaeoecol.*, **212**, 215–232.

Selvarengan, P., **Kubicki, J.D.**, **Guégan, J.** and **Châtellier, X.** (2010) Complexation of carboxyl groups in bacterial lipopolysaccharides: interactions of H^+, with Kdo and galacturonate molecules via quantum mechanical calculations and NMR spectroscopy. *Chem. Geol.*, **273**, 55–75.

Shirai, K., **Schöne, B.R.**, **Miyaji, T.**, **Radarmacher, P.**, **Krause, R.A.** and **Tanabe, K.** (2014) Assessment of the mechanism of elemental incorporation into bivalve shells (*Arctica islandica*) based on elemental distribution at the microstructural scale. *Geochim. Cosmochim. Acta*, **126**, 307–320.

Small, T.D., **Warren, L.A.** and **Roden, E.E.** (1999) Sorption of strontium by bacteria, Fe (III) oxide, and bacteria - Fe (III) oxide composites. *Environ. Sci. Technol.*, **33**, 4465–4470.

Sotaert, K., **Hofmann, A.F.**, **Middelburg, J.J.**, **Meysman, F.J.R.** and **Greenwood, J.** (2007) The effect of biogeochemical processes on pH. *Mar. Chem.*, **105**, 30–51.

Staudigel, P.T. and **Swart, P.K.** (2016) Isotopic behavior during the aragonite-calcite transition: implications for sample preparation and proxy interpretation. *Chem. Geol.*, **442**, 130–138.

Sutherland, I.W. (2001) Biofilm exopolysaccharides: a strong and sticky framework. *Microbiology*, **147**, 3–9.

Swart, P.K. (2015) The geochemistry of carbonate diagenesis: the past, present and future. *Sedimentology*, **62**, 1233–1304.

Tucker, M.E. and **Bathurst, R.G.C.** (1990) *Carbonate Diagenesis*. Blackwell Scientific Publications, Wiley-Blackwell, Hoboken, NJ, 320 pp.

Uroz, S., **Calvaruso, C.**, **Turpault, M.P.** and **Frey-Klett, P.** (2009) Mineral weathering by bacteria: ecology, actors and mechanisms. *Trends Microbiol.*, **17**, 378–387.

Van Lith, Y., **Warthmann, R.**, **Vasconcelos, C.** and **McKenzie, J.A.** (2003) Microbial fossilization in carbonate sediments: a result of the bacterial surface involvement in dolomite precipitation. *Sedimentology*, **50**, 237–245.

Vasconcelos, C. and **McKenzie, J.** (1997) Microbial mediation of modern dolomite precipitation and diagenesis under unoxic conditions (Lagoa Vermelha, Rio de Janeiro, Brazil). *J. Sed. Res.*, **67**, 378–390.

Walker, J.C. (1984) Suboxic diagenesis in banded iron formations. *Nature*, **309**, 340–342.

Watabe, N. (1965) Crystal-matrix relationships in the inner layer of mollusk shells. *J. Ultrastruct. Res.*, **12**, 351–370.

Weiner, S. and **Addadi, L.** (1991) Acidic macromolecules of mineralized tissues: the controllers of crystal formation. *Struct. Chem.*, **16**, 252–256.

Weiner, S. and **Addadi, L.** (2011) Crystallization pathways in biomineralization. *Annu. Rev. Mater. Res.*, **41**, 21–40.

Williams, D.F., **Arthur, M.A.**, **Jones, D.S.** and **Healy-Williams, N.** (1982) Seasonality and mean annual sea surface temperatures from isotopic and sclerochronological records. *Nature*, **296**, 432–434.

Wilson, P.A. and **Opdyke, B.N.** (1996) Equatorial sea-surface temperatures for the Maastrichtian revealed through remarkable preservation of metastable carbonate. *Geology*, **24**, 555–558.

Wiltshire, K.H., **Malzahn, A.M.**, **Wirtz, K.**, **Greve, W.**, **Janisch, S.**, **Mangelsdorf, P.**, **Manly, B.F.J.** and **Boersma, M.** (2008) Resilience of North Sea phytoplankton spring bloom dynamics: an analysis of long-term data at Helgoland Roads. *Limnol. Oceanogr.*, **53**, 1294–1302.

Wright, D.T. and **Wacey, D.** (2005) Precipitation of dolomite using sulphate-reducing bacteria from the Coorong Region, South Australia: significance and implications. *Sedimentology*, **52**, 987–1008.

Yang, C., **Rodionov, D.A.**, **Li, X.**, **Laikova, O.N.**, **Gelfand, M.S.**, **Zagnitko, O.P.**, **Romine, M.F.**, **Obraztsova, A.Y.**, **Nealson, K.H.** and **Osterman, A.L.** (2006) Comparative genomics and experimental characterization of N-acetylglucosamine utilization pathway of *Shewanella oneidensis*. *J. Biol. Chem.*, **281**, 29872–29885.

Zeebe, R. and **Wolf-Gladrow, D.** (2001) *CO2 in Seawater: Equilibrium, Kinetics, Isotopes. Elsevier Oceanography Series*, vol. **65**. Elsevier Science, Amsterdam, 346 pp.

Zhao, J.S., **Manno, D.**, **Beaulieu, C.**, **Paquet, L.** and **Hawari, J.** (2005) *Shewanella sediminis* sp. nov., a novel Na+-requiring and hexahydro-1,3,5-trinitro-1,3,5-triazine-degrading bacterium from marine sediment. *Int. J. Syst. Evol. Microbiol.*, **55**, 1511–1520.

Manuscript received 9 March 2017; revision accepted 17 October 2017